Generic comparison of lumen nucleation and fusion in epithelial organoids with and without hydrostatic pressure

Linjie Lu[†1-4], Kana Fuji[†5], Tristan Guyomar[1-4], Michèle Lieb[1-4], Marie André[1-4], Sakurako Tanida[5-7], Makiko Nonomura[8], Tetsuya Hiraiwa[9,10, 5], Yara Alcheikh[12], Siham Yennek[11], Heike Petzold[12], Cecilie Martin-Lemaitre[13], Anne Grapin-Botton*[12,14], Alf Honigmann*[12-14], Masaki Sano*[15,5], Daniel Riveline*[1-4]

[1]Institut de Génétique et de Biologie Moléculaire et Cellulaire, Illkirch, France
[2]Université de Strasbourg, Illkirch, France
[3]Centre National de la Recherche Scientifique, UMR7104, Illkirch, France
[4]Institut National de la Santé et de la Recherche Médicale, U964, Illkirch, France
[5]Universal Biology Institute, Graduate School of Science, The University of Tokyo, Tokyo, Japan
[6]Research Center for Advanced Science and Technology, The University of Tokyo, Tokyo, Japan
[7]Department of Aeronautics and Astronautics, School of Engineering, The University of Tokyo, Tokyo, Japan
[8]Department of Mathematical Information Engineering, College of Industrial Technology, Nihon University, Chiba, Japan
[9]Mechanobiology Institute, Singapore, National University of Singapore, Singapore
[10]Institute of Physics, Academia Sinica, Taipei, Taiwan
[11]The Novo Nordisk Foundation Center for Stem Cell Biology, Copenhagen, Denmark
[12]Max Planck Institute of Molecular Cell Biology and Genetics, Dresden, Germany
[13]Technische Universität Dresden, Biotechnologisches Zentrum, Center for Molecular and Cellular Bioengineering (CMCB), Dresden, Germany
[14]Cluster of Excellence Physics of Life, TU Dresden, 01062 Dresden, Germany
[15]Institute of Natural Sciences, School of Physics and Astronomy, Shanghai Jiao Tong University, Shanghai, China
[†]**Joint first authors**
***Corresponding authors: botton@mpi-cbg.de, alf.honigmann@tu-dresden.de, sano.masaki@sjtu.edu.cn, and riveline@unistra.fr**

Abstract: *Many internal organs in the body harbor a fluid-filled lumen. The mechanisms of lumens initiation and fusion have been reported as dependent on organ-type during organogenesis. In contrast, the physics of lumen suggests that force balance between luminal pressure and cell mechanics could lead to conserved rules which may unify their self-organisation. However, this hypothesis lacks experimental evidence. Here we compare lumen dynamics for three different systems (MDCK cysts, pancreatic spheres, and epiblast cysts) by using quantitative cell biology, microfabrication and theory. We report that initial cell number determines the maximum number of lumens but does not impact the steady state which is a final single lumen. In addition, lumen numbers exhibit two phases over time, a nucleation phase followed by a fusion phase. In the nucleation phase, lumens form between two cells in pancreatic and MDCK cysts whereas they form at the rosette stage between ten cells in epiblasts. In the second phase, lumens fuse by an increase in lumen volume for pancreatic spheres and MDCK cysts, whereas cell convergent directional motion leads to lumens fusion in epiblasts. We show that these phenomena are associated to the luminal hydrostatic pressure. We support these results with theoretical arguments and numerical simulations. We finally use MDCK cysts to manipulate cell adhesion and lumen volume and we successfully* reproduce the fusion dynamics of pancreatic spheres and epiblasts. Our results reveal self-organisation rules of lumens across systems with relevance for morphogenesis during development and for the design of synthetic *organs.*

Introduction.

Organogenesis relies on individual cells that proliferate and interact to self-organise. An interplay between the physical properties of cells, their tissue organisation, gene expression, and molecular control sets the complex rules for morphogenesis[1,2]. The cells in different organs use common means of controlling cell division, cell volume and shape, cell rearrangement and migration to enable different shapes to emerge[3]. Basic physical parameters of cells, such as pressure differences or surface tension, are crucial to the process. Understanding the physics of organogenesis requires clarifying these generic rules applicable to different cell types.

We took a generic approach to study the dynamics of a central structure in organs, *i.e.,* the lumen. Although lumen formation occurs in different epithelial organ models, several mechanisms of lumen formation are conserved across multiple systems such as hollowing after cell division[4–8] or by apoptosis leading to cavitation[7–9]. In addition, theory for the physics of lumen was proposed[10,11] and some physical mechanisms for its dynamics were reported experimentally[12,13]. A systematic comparison between cellular systems is lacking so far.

Here, we probed self-organisation of lumens on *in vitro* models. We use epithelial organoids as paradigms for lumen dynamics with physiological relevance[14–19]. We report a universal trend in various model systems, *i.e.* an increase in the number of lumens as a function of time followed by a decrease due to fusion until they all reach a single lumen. We also show that epithelial-derived lumens nucleate either after cell division or upon cell contact whereas epiblasts form lumens when they reach a rosette stage of 10 cells. By contrast, fusion of lumens is dominated by increase in pressure for pancreatic and MDCK spheres, whereas epiblast lumens fuse by cell motion. We show that epiblast lumens have negligible hydrostatic pressure in contrast to MDCK and pancreatic spheres. These rules are substantiated with a numerical simulation reproducing cell dynamics and lumen appearance using a phase field approach and by theoretical arguments. To further test these mechanisms, we used MDCK cysts to manipulate adhesion and lumen volume and we successfully reproduce the fusion dynamics of pancreatic spheres and epiblasts.

Results.

Distinct phases of lumen dynamics

To track the growth and morphology of organoids (Fig. 1), we designed a microwell-containing device optimized for cell imaging and cyst tracking by using soft lithography[20] (Fig. 1a and Materials and Methods). Single devices contained microwells of different diameters adjusted to the measured mean cell dimension of each cellular system and a constant height equal to the cell height (Ext. Fig. 1). This allowed us to follow different initial cell numbers over time within the same experiment, *i.e.,* 1, 2, 3, 4, 8, 16 cells (Fig. 1c). We used an MDCK cell line which expressed markers for cell-cell junctions and for lumens (see Materials and Methods) and this allowed us to track in three dimensions the number of lumens as a function of time in three dimensions (Fig. 1b-e). We observed two phases, Phase I with an increase in the number of lumens during the first 24 hours followed by Phase II with a decrease over time eventually reaching a single lumen. This suggests that cells formed new lumens over time and that these lumens underwent fusion irrespectively of their initial number. During Phase II, these lumens

86 could also undergo fusion irrespectively of their initial number and cyst shape (Fig. 1f,g). In addition,
87 larger initial cell numbers correlated to larger number of lumens, ranging from a peak of 1 lumen for 1
88 initial cell at 24 hours to 6 lumens on average for 16 initial cells. They reached single lumen within 24
89 hours (1 day) for 1 initial cell and 192 hours (8 days) for 16 initial cells.

90 We further explored whether this biphasic behavior was conserved in other systems. We plated
91 pancreatic cells freshly isolated from fetal mouse pancreases at 13.5 days of development in the micro-
92 cavities with adjusted dimensions and we tracked the evolution of lumen number over time (Fig. 2a and
93 Fig. 2b). We quantified these dynamics (Fig. 2b) and we found a biphasic trend similar to the MDCK
94 system (Fig. 1e). However, the distribution ranged from a peak of 1 lumen for 1 initial cell at 16 hours to
95 5 lumens on average for 16 initial cells. Lumens fused into a single lumen within 24 hours and 48 hours
96 respectively. The same experiment with epiblasts led to similar conclusions (Fig. 2c and Fig. 2d): the
97 lumen numbers increased and then decreased reaching single lumens, ranging from an average peak of
98 1 lumen to 4 lumens for initial cell numbers of 1 cell and 16 cells respectively. Lumen fusion into a single
99 lumen happened within 2 days and 3 days respectively. Altogether all systems exhibited the same
100 qualitative behavior, increase in lumen number with increasing initial cell numbers, and an increase of
101 lumens number followed by fusion leading to single lumens.

102 The three systems exhibited similar phases but with a different timing. We hypothesized that this may
103 be due to different cell cycle lengths of the different cell types. We thus plotted the number of lumens
104 per cell cycle as a function of initial cell number for each system (Fig. 3a). Remarkably, the curves were
105 similar for MDCK cysts and pancreatic spheres with an increase of 0.2 lumen per cell cycle per initial cell
106 number. In contrast, the slope was 5 times smaller for epiblasts, suggesting differences in the nucleation
107 mechanisms. Following the dynamics of MDCK cells we could see that lumens formed by two
108 mechanisms (Fig. 3b and Movie 1). As described previously, cells nucleated a lumen in the middle of the
109 cell-cell contact after cell division[6,21] (see time 1:40 top Fig. 3b and Ext. Fig. 3a). In addition, we found
110 that two cells formed a lumen when they adhered to each other (see time 2:00 bottom Fig. 3b and
111 Movie 2). The time needed for lumen appearance was similar between both processes (Fig. 3c). Both
112 mechanisms were also observed in pancreatic cells (Fig. 3d, Movie 3 and Movie 4) with the same 2 hours
113 timescale typically required to nucleate a lumen (Fig. 3e). It is worth noting that the low number of
114 lumens per cell cycle per initial cell number suggests that lumens are nucleated during this Phase I but
115 also undergo fusion with other lumens. The mechanism of nucleation was in sharp contrast with the
116 appearance of lumens in the epiblasts (Fig. 3f and Fig. 3g): the lumen nucleated only when a critical
117 number of about 10 cells formed a rosette (see time 48h in Fig. 3f and Fig. 3g and Ext. Fig. 3b and c). This
118 may explain the distinct dynamics in Phase I.

119 **Hydrostatic pressure driving lumen fusion in epithelial models**

120 The decrease in lumen number seen over time in Phase II suggested that lumen disappeared by fusing
121 together (Fig. 4a). Live imaging enabled us to observe and quantify lumen fusion. We plotted the lumen
122 fusion per cell cycle as a function of initial cell number (Fig. 4a). Unlike for Phase I, the three systems
123 exhibited different fusion rates. The fusion was the fastest in pancreatic spheres with a reduction of
124 lumen at a rate of 0.1 per cell cycle per initial cell number, followed by the epiblasts with a reduction of
125 0.08 per cycle per initial cell number. In contrast the decrease was about 3-fold slower smaller for MDCK
126 lumens fusions than for the other organoids. To further compare the systems, we followed the dynamics
127 of fusion of cysts for initial conditions of 8 cells until cysts reached similar dimensions and cell numbers

128 (Fig. 4b). MDCK cysts exhibited a striking dynamic: the nearest neighbouring lumens coming to contact
129 fused by breaking the cellular junctions separating them over 60 hours (Fig. 4b and Movie 5). We
130 quantified these dynamics by plotting the lumen index (LI) per lumen; LI quantifies the ratio between
131 the luminal area and outer cyst area to capture the respective increase in lumen volume (Fig. 4c, see
132 Materials and Methods). The LI of one lumen increased whereas the LI of the neighbouring lumens
133 decreased in the period preceding the fusion. This sequence of events was similar for pancreatic sphere
134 fusion but with faster kinetics (Fig. 4b and Movie 6) as evidenced in the LI quantification (Fig. 4d). In
135 contrast, when we tracked the fusion of epiblasts lumens (Fig. 4b and Movie 7) we did not see a
136 significant increase in the LI as illustrated by a constant LI prior to fusion (Fig. 4e). The large LI
137 (approximately 1) for pancreatic spheres may suggest that the luminal pressure is larger than the MDCK
138 sphere which presents a lumen index of 0.3 which is again 3-fold higher than the epiblast LI (see Ext. Fig.
139 4c). This indicates that increase in luminal pressure is large and important in pancreatic and in MDCK
140 spheres. If hydrostatic pressure is a driver of fusion, we reasoned that it must rip apart the adhesion
141 between cells separating two lumens. To gain insight into adherens junctions, we quantified the levels of
142 E-cadherins levels at junctions (see Fig. 5ab and Ext. Fig. 5c). The mean concentration of E-cadherin was
143 much larger for MDCK spheres compared to the other systems, which suggests that adhesion force may
144 counteract lumen fusion via luminal pressure in this system. This difference in adhesion was further
145 supported by inflation experiments where the cell layer was more easily disrupted in epiblast than in
146 MDCK spheres (Ext.Fig. 5d). This feature can explain the lower slope for the lumen fusion for MDCK cysts
147 compared to pancreatic spheres which may be dominated by large luminal pressure and low adhesion
148 (Fig. 4a).

149 To test this central role for luminal hydrostatic pressure, we performed drainage experiments designed
150 in our former study[22](see Materials and Methods, Ext. Fig.6 and Fig. 5d-g). By cutting locally the cell
151 layer with a laser, we could evaluate the luminal hydrostatic pressure associated to each cyst. Our
152 results show that MDCK cysts have a hydrostatic pressure of 65Pa, larger than pancreatic spheres[23], in
153 contrast to epiblast which have a hydrostatic pressure close to 0Pa. We also tested that the mechanical
154 properties of monolayers were similar (Ext. Fig. 7), supporting the notion that luminal pressure was the
155 driving force for nucleation and fusion of lumens.

156 **Motion-directed lumen fusion in epiblasts**

157 Since the slope of lumen fusion was much lower for MDCK cysts than pancreatic spheres and epiblasts,
158 we sought for an alternative mechanism driving lumen fusion. The lumen index value of epiblasts
159 suggests that luminal pressure does not play a key role in the fusion. In particular the neighbouring
160 rosettes compacted into a sphere in epiblasts (Fig. 4b) and this was associated to the transformation of
161 the outer layer of the cyst from an elongated shape to a sphere (Fig. 4i) in contrast to MDCK fusion case
162 where the cyst remained spherical (Fig. 4f). We then measured the distance gained along the long axis
163 of the cyst by cells: they corresponded to the distance needed for the lumens to fuse (Fig. 4j,k, see
164 Materials and Methods). This is in sharp contrast with MDCK cysts (Fig. 4g,h). These experiments suggest
165 that lumens fusion in epiblasts are driven by cells convergent directional motion associated with
166 changes in cyst shape, whereas lumens fusions are mainly mediated by luminal pressure for MDCK cysts
167 and pancreatic spheres.

168 **Toward quantitative generic rules for lumen dynamics**

We turned to numerical simulations to reveal the rules in cell proliferation, cell adhesion, lumen formation and luminal pressure, which could reproduce the main results across systems. These *in silico* experiments enabled us to test the hypotheses derived from our observations. In this context, we selected the phase field model which captures the complex dynamics of cells and lumens once a proper free energy is set[24–26]. We assumed that cells grow and divide at threshold time and volume and form a lumen (Fig. 5a) and we modulate the increase in lumen volume and control cell-cell adhesion (see Suppl. Note). In silico experiments evolve spontaneously by setting the initial conditions as in the real experiments. We illustrate typical evolutions of the numerical cysts with 8 cells as initial cell number with the knowledge of the respective proliferation time of our systems, the same doubling time for MDCK and pancreatic spheres and stronger adhesion force for MDCK cells (Fig.5). We obtained phenotypes similar to MDCK cysts (Fig. 6b blue, see also Movie 9); for larger luminal pressure with the same proliferation time (green), fusion looked similar to pancreatic spheres (Movie 10). Quantifications of lumen index in the numerical cysts for each case reproduced also the quantifications of experimental lumen index (compare Fig. 6d with Fig. 4c). Finally, to further validate the relevance of our simulations to experimental data, we quantified the dynamics *in silico* of the systems from initial stages by counting the number of lumens as a function of time. Strikingly we could reproduce the biphasic behaviour for all systems (Fig. 6c). These simulations support the importance of the interplay between cell proliferation, cell adhesion and luminal growth in setting quantitatively lumen dynamics across systems.

Based on our result of zero luminal pressure for epiblasts, we turned to alternative mechanisms. We analytically evaluated the number of cells needed to nucleate a lumen in the absence of hydrostatic pressure by assuming a similar free energy with the phase field model (Fig. 6e-h and Supplementary note). Our results show that 10 cells are needed to nucleate a lumen (see Fig. 6e,f) in good agreement with our results for epiblasts whereas 2 cells are sufficient for a cyst with luminal pressure (Fig.6g and 6h). This difference substantiates the differences between MDCK/pancreatic spheres on the one hand and epiblasts on the other hand.

Testing the model in MDCK cysts and epiblasts

Our modeling and experimental observations suggested that lumen growth, adhesion between cells and cellular properties governed the differences between the three systems. We further tested this experimentally using the MDCK system as a reference and perturbing these parameters. To evaluate the role of lumen growth in fusion, we prepared MDCK cysts with two lumens and we designed an inflation experiment using a micro-pipette to inject fluid[22] (Fig. 7a and Ext. Fig. 8). To show the fusion, we used dextran in the pipette. We could induce the fusion within minutes. This suggests that an increase in lumen growth rate can drive fusion of MDCK lumen faster than it normally takes, along the result of a faster response promoted by an increase of lumen volume in pancreatic spheres. In contrast, epiblast could not sustain this volume change upon injection, leading the whole structure to collapse instead of triggering fusion (Ext. Fig 9). The same enhanced fusion was obtained by an osmotic shock (Fig. 7b and 7c and Materials and Methods). In addition, the apparent role of cell-cell adhesion for MDCK cysts was further tested by simultaneously decreasing cadherin-mediated adhesion by chelating calcium with EDTA and using an anti E-cadherin blocking antibody[27,28] (Fig. 7d). We observed that lumen number is significantly decreased, suggesting that lumen fusion was facilitated (Fig. 7d, e). This suggests that adhesion between cells is an impediment to fusion in MDCK cysts. In addition, we tested the behaviour of E-cadherin KO MDCK cell line for 8 cells and 16 cells initial conditions: the biphasic behaviour was reproduced but this E-cadherin cell line presented a faster fusion (see Fig. 7f,g,h). This further confirms

212 that adhesion between cells can prevent fusion. Finally, to test the impact of cellular properties on
213 lumen formation, we used a MDCK cell line in which the tight junction proteins ZO1 and ZO2 were
214 knocked-out[22,29]. This cell line was shown to have smaller LI due to increased apical contractility[22] and
215 resembled the epiblast case with smaller lumen and elongated cells (see Ext. Fig. 10a). We initiated the
216 MDCK ZO-1/2 KO2 KO cysts with 1 to 16 cells and we repeated the observation of the number of lumens
217 as a function of time and initial cell numbers (Fig. 11a, b). The results show that fusion was facilitated in
218 the ZO-1/2 KO cyst. Several features of this ZO-1/2 KO MDCK cyst corresponded with epiblasts cysts,
219 such as low LI and similar mechanical response to inflation (Ext.Fig. 10b), as well as facilitated fusion as a
220 function of cell number. This suggests that tight junction deletion contributes to faster fusion. These
221 experiments of MDCK cysts transformations with mechanical or biological perturbations support the
222 notion that lumen fusion generically results from this interplay between luminal pressure and
223 mechanical cell interactions.

224 Finally, to show that activity was required for the fusion in the case of epiblasts, we recorded the fusion
225 of epiblasts in the presence of the myosin inhibitor, blebbistatin (Fig. 8a). Fusion was prevented, which
226 shows that active forces are needed to promote fusion. This was also obtained when adhesion was
227 reduced in MDCK ZO-1/2 KO (Ext. Fig. 10c). To further substantiate these fusion mechanisms with no
228 pressure, we prepared numerical epiblasts similar to the experimental system with two lumens and
229 small luminal pressure (Movie 11) with an elongated configuration similar to the experimental case
230 (compare Fig. 4b). Based on experimental measurements in this configuration (Fig. 4i-k), we imposed
231 radial cell motion by adding active forces (Fig. 8b) and we successfully recapitulated the fusion (Fig. 8c)
232 as well as cell motion within the cyst (Fig. 8d,e) and axis ratio of the cyst (Fig. 8f).

233

234 **Discussion.**

235 We have shown that the number of lumens depends on the initial cell number and their evolution
236 exhibits similar biphasic behaviours for MDCK, pancreatic spheres and epiblasts (Fig. 7). The nucleation
237 phase is dictated mainly by appearance of new lumens whereas the second phase is dominated by
238 fusion to reach a single lumen for all systems. Nucleation mechanisms are shared between MDCK cells
239 and pancreatic spheres both when cells divide and when two cells adhere to each other, whereas
240 epiblasts need about 10 cells to nucleate a lumen. MDCK and pancreatic spheres fusions are
241 predominantly driven by an increase in lumen index and high pressure, whereas fusion is determined by
242 active cell motion in epiblasts with low lumen index and negligible pressure. Our experimental
243 perturbations of MDCK fusions suggest that luminal pressure in competition with cell-cell adhesion
244 controls fusion. In pancreatic spheres the lumen index is larger than the MDCK cysts and fusion is likely
245 driven by luminal ion pumping, whereas epiblasts fusions are dominated by cells motion.

246 The mechanism of lumen nucleation after cell division has been reported for MDCK cells[6,30,31]. It is
247 consistent with the nucleation mechanism we report for MDCK and we report it for pancreatic spheres.
248 In addition, we also add the lumen nucleation associated to contact between cells as well, which
249 supports the notion that several mechanisms of lumen nucleation could co-exist with similar timing. It is
250 worth noting that lumen nucleation was reported in an assay between a cadherin coated surface and a
251 single cell[32] suggesting that adherens junctions formation between cells *per se* could trigger lumen
252 formation. Finally, we report that the larger number of cells is needed to nucleate a lumen in epiblasts

253 and it is consistent with Shahbazi *et al*[33,34]. Despite these multiple mechanisms for lumen nucleation, we
254 report and explain in a unified way the mechanisms for the nucleation, i.e. Phase I, across systems.

255 We distinguish fusion between lumens triggered by ion-pumping mechanisms leading to an effective
256 increase in hydrostatic pressure of the lumen in competition with cell-cell adhesion and fusion between
257 lumens triggered by cell re-organisation. This difference can be understood by a simple force balance
258 argument: when the lumen index is large, the hydrostatic pressure of the lumen pushes the cell apical
259 side and the cell monolayer thereby competing with cell-cell contacts; in contrast, when lumen index is
260 low, the hydrostatic pressure of the lumen is low and interactions between cells essentially determine
261 the potential fusion between lumens. Lumen fusion by increased osmotic pressure was reported in
262 various situations *in vitro* and *in vivo*[12,35,36] along our observations and this illustrates that common rules
263 of self-organisation across systems could determine the morphogenesis of organs in 3D.

264 It is interesting to understand why epiblasts show very low hydrostatic pressure. We note that MDCK
265 cysts and pancreatic spheres are sealed in the sense that Dextran cannot enter the luminal space[22,23].
266 This is in sharp contrast with epiblasts[34,37]. We propose that this difference is associated with low
267 luminal pressure. In addition, we conjecture that this property is associated to tight junction maturation,
268 *i.e.* tight junctions are fully matured in MDCK cysts whereas they do not reach this state in epiblasts. This
269 proposition is consistent with the similar lumen dynamics exhibited by epiblasts and by ZO-1/2 KO
270 MDCK cell lines. Future experiments will be needed to identify the molecular mechanisms associated to
271 tight junction maturation.

272 We propose that these nucleation and fusion mechanisms could be tested on other organoid systems.
273 The timing of cell proliferation compared to lumen fusion dynamics could be tuned to optimize the
274 target size of the organ with the relevant cell number and the number and size of lumens. Systems may
275 select fast pumping like the pancreas to allow multiple lumens to fuse rapidly with potential change in
276 luminal pressure to form a single duct[38]. By contrast, systems that would need to keep compartments
277 such as the thyroid gland may have developed larger adhesion properties to prevent fusion and allow
278 each zone to keep potential differences in composition[39].

279 In considering functional differences between cells connected to lumen dynamics, it is interesting to
280 note that cells change their states in the case of epiblasts[40]. From stem cells, they exit from pluripotency
281 and follow paths of differentiation leading to the right localization in the final organs. We propose that
282 this orchestration of proliferation with lumens nucleation and fusion could also be optimized to
283 generate organs with the relevant shape and cell numbers but also with the correct cell-state
284 distributions. Future experiments coupling our approach with spatial transcriptomics will allow to test
285 this hypothesis.

286 Our results could shed light on the synthesis of artificial organs. Indeed, it was reported that cell printing
287 was a promising method to generate organs[41,42]. Our results show that the cell number at plating, their
288 growth rates, and their fusions, contribute to the dynamics of the organs formation. This initial condition
289 correlates with morphology and functions of organ. As a result, a due care to the force balance would
290 need to be evaluated in the synthesis of organs and our framework with its numerical simulations could
291 serve as a solid basis to predict the future shape of the targeted organs.

292

293

294

295

296

297

298 **Acknowledgements.**

299 We thank the Riveline group for help and discussions and Erwan Grandgirard and the Imaging Platform
300 of IGBMC, Patrick Reilly for assistance in editing. We also thank Byung Ho Lee and Allison Lewis for
301 experimental, conceptual and image analysis advice and discussions. We thank Benoît Ladoux for
302 providing the MDCKII E- cadherin KO cell line. L.L. and T.G. are supported by HFSP and by the University
303 of Strasbourg and by la Fondation pour la Recherche Médicale. D.R. acknowledges the Interdisciplinary
304 Thematic Institute IMCBio, part of the ITI 2021-2028 program of the University of Strasbourg, CNRS and
305 Inserm, which was supported by IdEx Unistra (ANR-10-IDEX-0002), and by SFRI-STRAT'US project (ANR
306 20-SFRI-0012) and EUR IMCBio (ANR-17-EURE-0023) under the framework of the French Investments for
307 the Future Program. A.G.B, A.H., M.S. and DR acknowledge the Research Grant from Human Frontier
308 Science Program (Ref.-No: RGP0050/2018).

309 ------

310 **Materials and Methods.**

311 **Cell sources and expansion**

312 We used 3 cellular systems, MDCK II cell lines, mouse embryonic cells (mES cells)[43], and pancreatic
313 spheres[44]. Other mutant cell lines were used for MDCK: MDCK II E-cadherin-GFP/Podocalyxin-
314 mScarlett/Halo-CAAX[45], MDCK II ZO1/2-KO[22] and MDCK II E-cadherin KO[46].

315 The MDCK II cell lines were cultured in MEM (Gibco 410900028) with 5 % Fetal Bovine Serum (Sigma,
316 USA), 1mM Sodium Pyruvate (Gibco 11360-070) and 1x NEAA (Gibco 11140050). MDCKII cells were
317 resuspended every 2 to 3 days with trypsin-EDTA after they reached 70-95% confluency. A seeding
318 density of about $3*10^5$ cells per 75 cm^2 was used for sub-culture. R1 ES-cell line was used for the culture
319 of epiblast (quote 25). Mouse embryonic stem cells were expanded with 1:1 DMEM/F12 (ThermoFischer
320 31331028) and neurobasal medium (Gibco 21103049) supplemented with 1x N2 (Gibco 17502048), 1x
321 B27 (Gibco 12587010) and 1x NEAA (Gibco 11140050), 55µM 2-Mercaptoethanol (Gibco 21985023),
322 3µM CHIR 99021 (Sigma SML 1046-5mg) and 2x LIF produced at IGBMC-Strasbourg in non-adhesive
323 flasks[43]. Cells were sub-cultured every 4 days until the size of spheres reached a diameter of 80µm.
324 Pancreatic spheres were prepared from the dissection of E13.5 embryos (mouse CD1 from Charles River
325 Laboratory) using the protocol reported in Greggio et al[44] and used without passaging.

326 **Cells diameter measurement.**

327 For the three systems, single cells were plated after trypsinisation and labeled using 10nM SiR-actin
328 (TEBU-BIO, 251SC001). The middle planes of spherical cells were imaged. The associated surfaces were
329 measured with Fiji and the distributions of cells diameters were plotted (see Ext. Fig. 1). Cavities

330 diameters were designed accordingly by taking the mean value of each distribution to control the initial
331 cell numbers (Ext. Fig. 1c). All cavities had a cell height from 10µm to 17µm to keep the height similar to
332 one cell diameter.

333 **Microfabrication and cavity map.**

334 We designed the samples with a map of patterns for cavities in order to: (i) track the evolution of the
335 same cysts up to a week, (ii) test a large number of cysts with the same initial cell number and (iii) test
336 the effects of different initial cell numbers for the same biological repeat (see Fig. 1a). The same strategy
337 was adapted for each system by designing the cavity map accordingly.

338 Cavities were prepared using soft lithography as described in Bhat et al[20]. Briefly, we designed a mask
339 with
340 AutoCad to obtain a large number of motifs and different diameters. The motifs were selected to
341 contain many initial cells number conditions. We used the following calculation of the motif's diameter,
342 rescaled with the mean cell diameter: S(surface of cavities)= number of initial cells*surface of cells.
343 These designs were printed on photomask and then we transfer these patterns on SU-8 silicon wafer
344 with soft lithography. Next the design was replicated on a PDMS mold. Finally, these designs were
345 transferred to cover-glass which allows us to achieve higher resolution images.

346 **Cell seeding in microfabricated cavities for the control of initial cell number.**

347 To generate cysts and organoids in micro-fabricated cavities, we seeded cells in micro-cavities with the
348 following steps based on our former protocol[20,47]. Briefly, (i) the microfabricated-cavities on coverslips
349 were activated with O_2 plasma (Diener); (ii) substrates were incubated with 5µg/ml laminin (Sigma
350 11243217001) for 1 hour at room temperature followed by washing steps; (iii) cells in suspension were
351 centrifuged 3 times at 1000 rpm for 3 minutes on the samples to direct cells inside micro-cavities; (iv)
352 the coverslips were then rinsed gently to get rid of the excess of cells between cavities; (v) 15 µl Matrigel
353 (Corning, 356231) was added on top of the sample. After solidification of the Matrigel, the relevant
354 media were added depending on the cyst types. For pancreas spheres, single cells were dissociated from
355 the E13.5 pancreases and immediately seeded in the micro-well without centrifugation.

356 System-specific media were added to obtain pancreatic spheres or epiblasts. Pancreatic sphere was
357 formed by using DMEM/F12 (ThermoFischer 31331028) with B27 (Gibco 17504-044), recombinant
358 Human FGF2 (R&D 233-FB-025), Y-27632 (Sigma Aldrich ab120129) and Penicillin-Streptomycin (Gibco
359 15070-063)[44]. Epiblasts were differentiated by using 1:1 ratio of DMEM/F12 (ThermoFischer 31331028)
360 and neurobasal medium (Gibco 21103049) containing 0.5x N2 (Gibco 17502048), 1x B27 with vitamin A
361 (Gibco 12587010), 1x NEAA (Gibco17504044), 0.1mM 2-Mercaptoethanol (Gibco 21985023), 0.15mM
362 Sodium Pyruvate and 0.2mM LGlutamaine (Life Technology GmbH 11360039).

363 **Immunostaining.**

364 For immunostaining, we followed standard protocols Greggio, C. et al[45,48]. Briefly, samples were washed
365 with PBS and fixed with 4% paraformaldehyde (Electron Microscopy Sciences 15710) diluted in PBS for
366 15 minutes. Cells were permeabilized with 0.5% Triton-X-100 for 15 minutes and then a blocking
367 solution made of 1% Normal Goat Serum in PBS 1X was added overnight. Primary antibodies were

368 added directly to the blocking solution for two days at 4°C. Following 3 successive washing steps with
369 PBS, the samples were stained with the relevant secondary antibodies for 2 hours at room temperature.
370 We used the following primary antibodies: Anti-E-cadherin (Abcam, Ab11512 and Ab53033), Mouse
371 monoclonal Anti-Podocalyxin (BIO-TECHNE SAS, MAB1556-SP), Alexa Fluor Phalloidin 488
372 (ThermoFisher, A12379) for F-actin and DAPI (Sigma MBD0015) for the nucleus. Samples were washed
373 three times in PBS and mounted on a home-made sample holder system for imaging and conservation.

374

375 **Microscopy.**

376 In order to track the number of lumens in MDCK cysts, MDCK cells expressing Ecad – Podxl were used to
377 visualize adherens junctions and apical side, respectively. After cell seeding, images were taken at an
378 interval of 24 hours using Leica DMI8 with an Evolve 512 camera coupled to a spinning disk microscope
379 (CSU W1) with a 25x water objective (NA = 0.9) and 63x glycerol objective (NA = 1.2) using the software
380 Metamorph for image acquisition. Positions were chosen based on initial cell numbers and the same
381 MDCKII cysts were acquired in 3D every 24h. This was possible with the cavity map reported above. For
382 pancreatic spheres and epiblasts, initial conditions were controlled with the same method and samples
383 were fixed and stained with the relevant antibodies before 3D acquisition with the same microscopy
384 setup.

385 To record the lumen formation in MDCK, MDCK cysts were imaged at a time interval of 5 min for more
386 than 24 hours in a setup regulated for 5% CO_2 and 37°C temperature. We used MDCK cells stably
387 expressing E-cadherin-GFP and podocalyxin as readouts for cells junction and lumen. To record the
388 lumen nucleation in pancreatic spheres, we imaged them live after cells seeding with phase contrast
389 microscopy (Fig. 3d). For the characterisation of lumen nucleation in epiblasts, we fixed samples with
390 every 8 hours after cells seeding and we stained for E-cadherin and podocalyxin prior imaging (Fig. 3f).

391 For lumen fusion events in MDCK cysts, we used a 63x glycerol objective (N.A.= 1.2). Different organoids
392 were selected as starting positions and imaged every 30 min for up to 3 days. Z-stacks (60 µm range, 1
393 µm step) were acquired. For lumen fusion in epiblasts, epiblasts were imaged from day 2 with SiR-actin
394 (TEBU-BIO, 251SC001) after 1 hour incubation before the experiment. Then SiR-actin mix were
395 incubated with media leading to a final concentration of SiR-actin and Verapamil. The concentrations
396 were larger for MDCK cysts for optimal visualisation. Lumen interaction events were recorded with a
397 Leica CSU-W1 spinning disk (63× objective) for more than 10 hours at an interval time of 30 min.

398 **Perturbation experiments.**

399 For the inflation experiment[22] (Fig. 7a), MDCK cysts were used after 5 days of culture. We first removed
400 gently Matrigel from the top of micro-wells with a needle. The lumen was inflated by flowing media
401 containing fluorescent dextran (Fisher Scientific SAS D22914) in the relevant media with a micro-pipette
402 and images were taken using Leica spinning disk equipped with micromanipulators. For osmotic shock,
403 we incubated the sample with 300 mM D-mannitol solution (Sigma M9546).To investigate the role of
404 adhesion in lumen fusion, we used 5 mM EDTA and E-cadherin 10 µg/ml antibody [27,28] (Fig. 7b).
405 Snapshots of MDCK cells were taken right before addition of EDTA/E-cadherin antibody and then the
406 cysts were acquired in 3D for 60 minutes to record the fusion events. To interfer with cell motion during

407 fusion in epiblasts, we used the myosin inhibitor blebbistatin (Sigma B0560) at 10 μM with a DMSO
408 sample for control. For the hydrostatic pressure measurement and lumen drainage, we used our
409 established method. Hydrostatic pressure was calculated based on the Hagen-Poiseuille model. Channel
410 dimensions were confirmed through combined fluorescence and transmission light imaging, ensuring
411 accurate assessment of channel size and pressure parameters[22,23]. Surface tension measurements were
412 based on established methods[49].

413

414

415 **Imaging and data analysis.**

416 To extract the shapes and measure the volumes and surfaces of lumens and organoids, we used LimeSeg
417 Fiji Plugin and Skeleton Seg. The segmented 3D structures were saved and visualized. Analysis and
418 quantification were performed with Paraviewer[50].

419 The number of lumens were rescaled with respect to the cell cycle (Fig. 3a and Fig. 4a) by dividing the
420 number of lumens by the duration of each cell cycle. We took 18h for MDCK, 18h for pancreatic spheres,
421 and 9h for epiblasts. We checked that doubling times were consistent with the number of cells counted
422 in each system. In addition, we define lumen as a fluid-filled cavity between cells within the optical
423 resolution together with accumulation of apical marker such as podocalyxin and F-actin. Lumen index is
424 defined as the ratio between the area of lumen and the area of the outer shell of the cyst. They were
425 measured for each system. The numerical lumen index was measured by taking 2D lumen surface over
426 cyst surface. To compare the fusion process between MDCK cyst and epiblast, we ellipse fitted the outer
427 contour of cysts to extract the long and short axis. Then, we plotted the major axis over the minor axis
428 as a function of time (Figure 4f,i). To characterize the associated cell motion during fusion, we plotted
429 cell trajectories by using tracking their centers (Figure 4h,k).

430 Data were plotted using a written Python code and GraphPad Prism. Statistical tests were performed
431 using non-parametric Mann-Whitney test (two-tailed) to evaluate the significance between lumen
432 formation after cell division and when cells met (Figure 3c,e), lumen occupancy (Fig. 5b), intensity of E-
433 cadherin (Fig 5c), and the difference of number of lumens between WT MDCK cyst and ZO-KO cyst
434 (Figure 6h). The differences of number of lumens before and after EDTA+ anti-E-cadherin treatment
435 were assessed for statistical significance by using Wilcoxon matched-pairs signed rank test (Figure 7e).
436 Differences between groups for the pipette inflation experiment were analysed for statistical
437 significance by ANOVA. Statistical significance was indicated using the following symbols: ns p-
438 value >0.05, * $p < 0.05$, ** $p < 0.01$ and *** $p < 0.001$.

439 The number of experimental repeats and number of cyst or organoids are indicated in the Figure
440 captions.

441 **Theoretical model and numerical simulations.**

442 The cyst was theoretically modeled based on the multi-cellular phase field model with lumen[25] but
443 additionally incorporating the extracellular matrix around the cyst. To carefully control the surface

tension of each entity (each cell, lumen, ECM), we applied the resharpening method proposed in Refs. [51,52], which enabled us to eliminate the surface tension artificially generated due to the construction principle of the phase field model. The details of this theoretical model are given in Supplementary Note Theory.

Materials, Data and Code availability.

All materials will be available upon reasonable request.

The Data are available upon request and the software Code used for the simulation is available in the Github, https://github.com/kana-fuji/MCPFM_for_Lumen_Fusion.git

----

Movies Captions.

Movie 1 - Lumen nucleation after cell division for MDCK cyst. MDCK cells expressing E-cadherin in green and Podocalyxin. Time in hh:mm:ss.

Movie 2 - Lumen nucleation after cells meet for MDCK cyst. MDCK cells expressing E-cadherin in green and Podocalyxin. Time in hh:mm:ss.

Movie 3 - Lumen nucleation after cell division for pancreatic sphere. Time in hh:mm.

Movie 4 - Lumen nucleation after cells meet for pancreatic sphere. Time in hh:mm.

Movie 5 - Lumen increase in volume leads to lumen fusion for MDCK cyst. MDCK cells expressing E-cadherin in green and Podocalyxin in red with 8 cells as initial conditions. Time in hh:mm.

Movie 6 - Lumen increase in volume leads to lumen fusion for pancreatic spheres. Pancreatic spheres were imaged with 8 cells as initial condition. Time in hh:mm.

Movie 7 - Centripetal motion with low lumen occupancy leads to lumen fusion in epiblast. Time in hh:mm.

Movie 8 - Simulation movie of typical numerical evolution of cysts.

Movie 9 - Simulation movie of lumen interaction and fusion for 8 cells condition – with a dynamic similar to MDCK cyst.

Movie 10 - Simulation movie of lumen interaction and fusion for 8 cells – with a dynamic similar to pancreatic sphere.

Movie 11 - Simulation movie of lumen fusion for 8 cells condition – with a dynamic similar to epiblast.

Figures Captions

475 **Figure 1 - Lumen nucleation and fusion in MDCK spheroids with controlled initial cell numbers.** a.
476 Mask for the design of the cavity map. Cavities of different diameters were arrayed and designed to
477 accommodate different initial cell numbers. b. Schematic representation of lumenogenesis. Dissociated
478 plated cells adhere to each other and then lumens (surrounded by red line) are nucleated and
479 eventually fuse. c. Typical dynamics of MDCK cysts forming from controlled initial cell numbers (E-
480 cadherin in green, Podocalyxin in red). Initial cell numbers are shown at time 0 in cavities (scale bar) and
481 the shapes of the same spheroids are captured every day. The yellow line outlines the zone of MDCK
482 cysts which reached the single lumen stage. Scale bar 10µm (N=3, n≥ 10). d. 3D visualization of four
483 lumens and spheroids corresponding to c and indicated as 1,2,3,4. left: 3D viewer of spheroids with E-
484 cadherin in green and Podocalyxin in red. Right: 3d viewer of lumen by Imaris. e. Quantification of the
485 number of lumens in MDCK spheroids as a function of time for different initial cell number: 1,2,3, 4, 8,
486 16 cells. Each point represents an individual cyst, while the dark line corresponds to the mean value, and
487 the shaded region indicates the standard deviation. The number of lumens increases over time and with
488 initial cell number. All cysts end up close to single lumens. (f,g) External control of MDCK cyst growth
489 using micro-well confinement. Comparison of lumen nucleation in circular and rectangular micro-wells
490 shapes varying initial cell numbers. Podocalyxin is labeled in red and E-cadherin is labeled in green. (g)
491 Representative images show cyst morphology at Day 0 (left) and Day 4 (right). Scale bars: 20µm in f and
492 in g.

493

494 **Figure 2 - Lumen nucleation and fusion in pancreatic and in epiblast spheres.** a. Typical evolution of
495 pancreatic spheres shapes as a function of initial cell number and time (F-actin in green, nucleus in
496 Magenta) (N=3, n>20). Scale bars 10µm at time 0 and at time 96 h with 3D zooms on outlined pancreatic
497 spheres. b. Quantification of the number of lumens in pancreatic spheres as a function of time for
498 different initial cell numbers: 1,2, 4, 8, 16 cells. c. Typical evolution of epiblasts as a function of initial cell
499 number and time (E-cadherin in green, Podocalyxin in red) (N=3, n>20). Scale bars 10 µm at time 0 and
500 at time 72 h with 3D zooms on outlined epiblasts. d. Quantification of the number of lumens in epiblast
501 as a function of time with different initial cell numbers, 1, 2, 4, 8, 16 cells. Each point represents an
502 individual cyst, while the dark line corresponds to the mean value, and the shaded region indicates the
503 standard deviation. For a and c, the yellow line outlines the zone with single lumens. For both systems,
504 the number of lumens increases as a function of time and with initial cell numbers. All cysts end up close
505 to single lumens. Note that the timescales are different for the 3 systems indicated with the same colour
506 code across the article (compare Fig. 2b, Fig. 2d and Fig. 1e).

507 **Figure 3 - Rules of lumen nucleation in the 3 systems.** The lumens are nucleated after cell division and
508 after cells meet in MDCK spheres and pancreatic spheres but they form after about 5 cell divisions in
509 epiblasts. a. Lumen nucleation per cell cycle as a function of initial cell numbers. The increase is linear
510 for the 3 systems. MDCK and pancreatic spheres have the same slope whereas epiblasts have a slope 5
511 times lower. b. Snapshots of lumen nucleation in MDCK cysts. Top: Lumen formation after cell division in
512 MDCK cysts (Movie 1) N=5, n=32. Bottom: Lumen formation after contacts between cells in MDCK cysts
513 (Movie 2) N=4, n=10 (E-cadherin in green and Podocalyxin in red). Time relative to the junction
514 formation set as time 0. Time in hh:mm. Scale bar 10 µm. c. Quantification of lumen appearance time
515 after cell division or after cells meet. d. Snapshots of lumen nucleation in pancreatic spheres, Top: lumen
516 formation after cell division, see also Movie 3. Bottom: lumen formation after two cells meet; see also
517 Movie 4. Time relative to the junction formation set as time 0. Time in hh:mm. Scale bar 10 µm. e.
518 Quantification of the lumen nucleation after cell division or after cells meet. f. Lumen nucleation in

519 epiblasts fixed at 8h, 16h, 24h, 32h, 40h and 48h after cell seeding, stained with DAPI in blue,
520 podoxalyxin in red and E-cadherin in green. g. Number of cells as a function of time. (N=2, n>10).
521
522
523 **Figure 4 - Rules of lumen fusion in the 3 systems.** MDCK and pancreatic spheres lumens fuse by
524 increasing the lumen index whereas epiblasts fuse by cell motion with low lumen index. a. Top: scheme
525 of lumen fusion corresponding to Phase II. Bottom: quantification for the speed of lumen fusion. The
526 plot represents lumen fusion per cell cycle as a function of initial cells number (mean value ± standard
527 error of the mean and the curve represent the fit of mean). Pancreatic spheres and epiblast display
528 faster lumen fusion than MDCK cysts. B. Lumen fusion across systems. Top: MDCK cyst (E-cadherin in
529 green and Podocalyxin in red, also see Movie 5). Middle: Pancreatic sphere (phase contrast images, also
530 see Movie 6). Bottom: epiblast (Sir-actin, also see movie 7). c-e. Comparison between lumen indices
531 (ratio of surface of lumen over the surface of cyst) for the three systems presented on panel b: MDCK
532 cyst (c), pancreatic sphere (d) and epiblast (e). For each system, the blue and black curves correspond to
533 individual lumen 1 and 2 on panel b. f-l. Characterization and comparison between cellular dynamics
534 and tissue morphology in MDCK cyst (top) and epiblast (bottom). f,i. Elongations of the cyst defined as
535 the ratio of long axis over short axis of the organoid as a function of time. g,h. Distance between the
536 center of cells and the center of cysts over time. During the fusion process, MDCK cells are at a constant
537 distance from the center of the cyst whereas epiblast cells move inwards. h,l. Single cells trajectories.
538 Time is indicated with color bar and red point indicate the last time point. Epiblast cells display
539 centripetal motion.

540 **Figure 5- Comparison between phenotypes and hydrostatic pressure in MDCK cysts, pancreatic**
541 **spheres and epiblasts**. a. Typical images of the 3 systems with readouts for E-cadherin in green and F-
542 actin in red. Scale bar 10 µm. b. Quantification of lumens index for the 3 systems. c. Comparison of E-
543 cadherin levels between the 3 systems defined as intensity of E-cadherin on the junction minus intensity
544 in the cytoplasm and normalised by the intensity of the background. **** corresponds to $p < 0.0001$.
545 (d) Measurements of hydrostatic pressure in MDCK cysts and epiblasts by laser cutting. Images show the
546 midplane cross-sections of cysts before and after laser cutting, with red segments indicating the
547 positions of cuts. (e) Estimation of hydrostatic pressure in the lumen using the Hagen-Poiseuille law (see
548 Methods). (f) Lumen volume changes over time following laser cutting. The dark line represents the
549 mean volume change, while the shaded region indicates the standard deviation. (g) Hydrostatic pressure
550 measurements show an average of 65 Pa in MDCK cysts and close to 0 Pa in epiblasts. Data are based on
551 three independent experiments (N=3), with 27 MDCK cysts (n=27) and 22 epiblast samples (n=22). Scale
552 bar: 10 µm.

553

554 **Figure 6 – Phase field model for the nucleation and fusion of lumens for the 3 systems.** a. The cells
555 increase in volume and divide when they reach a threshold volume or after a threshold time. A lumen is
556 formed after each division. The numerical cysts grow over time; see Movie 8 for typical numerical
557 evolution of cysts. b. The pressure Ksi and proliferation time are controlled and two conditions are
558 plotted as a function of numerical time. Each case corresponds qualitatively to each experimental
559 system, see also Movie 9 and Movie 10. c. Quantification of the number of lumens as a function of time.
560 The number of lumens increases and then decreases. These two subsequent phases are similar to the
561 experimental phases reported in Fig. 1 and in Fig. 2. d. Numerical lumen indices measured for the 2

562 conditions. Their dynamics are similar the 2 experimental dynamics reported in Fig. 4. e-i. e. Schematic
563 showing the correlation between pressure and lumen formation time. Left panel: lumen formation is
564 delayed in the absence of pressure; right panel: lumen nucleation can occur at the two-cell stage under
565 applied pressure. f-h. Free energy dependency as a function of lumen radius for distinct hydrostatic
566 pressure. (f) F(r, R_min) : (f) $\Delta p = 0$ [Pa] for N=2, 4, 8, 12. (g) $\Delta p = 30$ [Pa] for N=2, 4, 8, 12; and (h)
567 $\Delta p = 100$ [Pa] for N=2, 4, 8, 12. Numerical parameters are $\gamma_A = 100\ [Pa \cdot \mu m]$, $\gamma_L = 100\ [Pa \cdot \mu m]$,
568 $R_0 = 20\ [\mu m]$, $L = 40\ [\mu m]$, $L_0 = 38.5\ [\mu m]$, $k = 0.01$, $k_E = 0.02$ for all cases. For N=12 case, we
569 assumed regular dodecahedron shape for calculation.

570 **Figure 7 - Testing the fusion mechanisms with perturbation experiments on MDCK cysts**. Increasing
571 lumen size by injection or decreasing cells adhesion leads to faster to lumen fusion. a. Inflating MDCK
572 spheres with micropipette. E-cadherin in green and podocalyxin in red and Dextran in Magenta. Scale
573 bar: 20 µm. The inflation triggers the fusion between lumens. b. Effects of osmotic shock on MDCK cysts
574 with multiple lumens. Experimental setup (top left): MDCK cysts were cultured for 1 day before being
575 treated under control conditions or with D-mannitol. The culture duration is indicated in days.
576 Representative images of cysts are shown at two time points: day 1 (top right) and day 3 (bottom left)
577 for each condition. Cysts are stained for F-actin (magenta) to visualize structural changes. Scale bar: 10
578 µm. c. Statistical analysis based on three independent experiments (N=3), with 79 cysts in the control
579 group (n=79) and 198 cysts in the D-mannitol-treated group (n=198). $p < 0.0001$. d. Decrease in cells
580 adhesion leads to faster lumen fusion. Snapshot of timelapse with control (top) and EDTA + antibody
581 block (bottom). E-cadherin in green and podocalyxin in red. Scale bar: 10 µm. e. Quantification of
582 number of lumens after EDTA+antibody treatment. Two independent experiments. Statistical analyses: T
583 test. **** $p < 0.0001$; ns, not significant. (n control=15; n EDTA=16). e-g. Decreasing cell adhesion by
584 using MDCK E-cadherin KO. The comparisons between MDCK WT and E-cadherin KO cysts over time and
585 initial cell number in d (top two rows: 8 cells, bottom two rows: 16 cells). f. Quantification of the number
586 of lumens in WT and E-cadherin KO cysts as a function of time for the initial cell number 8 and 16 cells.

587 **Figure 8: Perturbation of lumen fusion in the epiblast.** (a) Representative images of the lumen fusion
588 process in the epiblast. The top panel shows the control condition treated with DMSO, and the bottom
589 panel shows the effect of blebbistatin treatment. Lumens are visualized with SiR-actin (gray). Scale bar:
590 5 µm. b-f. Numerical simulations for the fusion of epiblast-like cysts, see also Movie 11. b. Definition of
591 parameters for the fusion of epiblast-like cysts. c. Fusion of two lumens in epiblast-like condition. d. The
592 cell motions are tracked as well as the distance of cells with respect to the center of mass of the system
593 (e) and the change in aspect ratio of the cysts (f). The numerical dynamics correspond closely to the
594 experimental time evolution of the same measurements in epiblasts fusion, see Fig. 4j-l.

595 **Figure 9 – Comparison of lumen nucleation and fusion in organoids with/without hydrostatic**
596 **pressure. Row 1:** Pancreatic spheres, MDCK cysts and epiblasts have two phases for the number of
597 lumens as a function of time. **Row 2: Key differences in hydrostatic pressure observed between the**
598 **three systems. Row 3:** Nucleation rules are similar for pancreatic spheres and MDCK cysts, lumens form
599 after cell division and when two cells meet; in contrast, a minimum of about 10 cells are required for the
600 lumen nucleation of lumens in epiblasts. **Row 4:** Lumens fusion are similar between pancreatic spheres
601 and MDCK cysts but with distinct pumping rates. In pancreatic spheres, fast pumping leads the increase
602 in lumen index and subsequent fusion; in MDCK cysts, lower increase in lumen index leads the fusion. In
603 contrast, fusion occurs with centripetal cell motion in epiblasts with low lumen occupancies.

604

605 **Extended Figures Captions**

606 **Extended figure 1: Diameter measurement:** a. Middle plan of single cells for MDCK, mES, pancreatic
607 progenitor from top to bottom labeled with Sir-actin. b. Diameter distribution: N=3, n=(MDCK), n=(mES),
608 n= (pancreatic progenitor). Scale bar 5 µm. c. Selections of diameters for cavities for distinct cells.

609 **Extended Figure 2:** Examples of distributions for the number of lumens at the peak value at the end of
610 Phase I (Left) and at the end of Phase II at the single lumen stage (Right).

611 **Extended Figure 3**: **Lumen nucleation in MDCK cysts and in epiblasts.** (a) Lumen formation is identified
612 by the presence of a hole at the junction and the accumulation of the apical protein Podocalyxin. (b) Top
613 two-panel row: epiblasts showing accumulation of Podocalyxin without lumen formation, as no hole is
614 present at the junction. Bottom two-panel row: Lumen nucleation in epiblasts characterized by the
615 accumulation of Podocalyxin and the presence of a hole at the junction. c. 3D visualization of cell
616 counting in epiblasts. From left to right: 2D Cut: A cross-sectional view of the cells in 2D. 3D View with
617 DAPI Staining: A 3D visualization highlighting nuclear structures with DAPI staining. Center of Cells in 3D:
618 The central positions of cells in 3D space, marked in different colors to differentiate individual cells.
619 Merged View: A composite image that integrates the 3D DAPI visualization with the 3D cell centers.
620 Scale bar: 10 µm.

621 **Extended Figure 4*:* Lumen fusion dynamics across different systems**. (a) Representative examples of
622 lumen fusion in MDCK cysts, pancreatic spheres, and epiblasts, along with quantification of the lumen
623 index. Lumens with low and high lumen index are shown in blue and black, respectively, while the sum is
624 indicated in red. MDCK cysts are labeled with E-cadherin (green) and Podocalyxin (red), while pancreatic
625 spheres and epiblasts are visualized using SiR-actin (gray). Additional examples of lumen fusion are also
626 shown. (b) Quantification of lumen index in another set of examples across the three systems. (c) Mean
627 lumen index for each system, represented by the dark line, with the shaded region indicating the
628 standard deviation (N=3, n=3). Scale bar: 10 µm.

629 **Extended Figure 5: Adhesion is different between epithelial cysts.** (a) Immuno-staining of wild type
630 MDCK and MDCK cells overexpressing E-cadherin, scale bar 20 µm. Cyst are stained for F-actin
631 (magenta) and nucleus in cyan. (b) Western blots for E-cadherin comparing wild type MDCK cells, MDCK
632 cells overexpressing E-cadherins, and (c) epiblasts. (d) Micropipette inflation experiments on MDCK cysts
633 (left) and epiblasts (right) (see Mukenhirn et al, 2024[22]).

634 **Extended Figure 6: Association between lumen index and hydrostatic pressure.**
635 (a) Time-lapse images showing drainage triggered by a local laser cut in MDCK cysts, with the midplane
636 captured before and after the cut. The positions of the cuts are marked by red segments. Two
637 representative examples are shown, with time indicated in seconds (s). Scale bar: 10 µm. (see
638 Mukenhirn et al., 2024[22] for details). (b) Relationship between hydrostatic pressure and lumen
639 occupancy in MDCK cysts. (c) Laser-induced drainage experiment demonstrating changes in cyst
640 midplane over time, with the cut positions indicated by red lines. The volume of each lumen is
641 monitored throughout the experiment
642 (d) Volume changes in lumens over time, where different colors represent individual cysts. Smaller

643 lumens are depicted by blue circles, and larger lumens by black squares. (e) Corresponding hydrostatic
644 pressure differences for each experiment, with the color coding consistent with panel (d).

645 **Extended Figure 7: Surface tension measurement of MDCK cysts with single and multiple lumens.** (a)
646 Brightfield Images: Representative brightfield images show MDCK cysts undergoing surface tension
647 measurements, highlighting cysts with multiple lumens (top panel) and a single lumen (bottom panel).
648 Scale bar: 20 µm. (b) Box Plot Analysis: Data are presented as mean ± standard deviation (s.d.) with
649 individual data points overlaid, providing a view of both central tendency and data variability.

650 **Extended Figure 8: Micropipette inflation swelling experiments on MDCK cysts with two lumens.** The
651 left two panels show the cysts before injection, and the right two panels show the cysts after injection.
652 Each row represents an individual example. Cysts are labeled with E-cadherin (green), Podocalyxin (red),
653 and Dextran (magenta). The inflation procedure triggers lumen fusion. Scale bar: 10 µm.

654 **Extended Figure 9: Micropipette inflation assay in epiblasts and MDCK-II cysts.** Micropipette inflation
655 swelling experiments on epiblasts with two lumens. Top panels show the condition before injection, and
656 bottom panels show after injection, with three images corresponding to (left to right): dextran staining,
657 SiR-actin + dextran overlay, and transmission light microscopy. Scale bar: 10 µm.

658 **Extended Figure 10: Comparison between MDCK wild type, ZO1/ZO2 KO cysts and epiblasts.** a. Cell-cell
659 contacts and lumens are stained with E-cadherin (in green) and F-actin (in red), scale bar: 5 µm. Note
660 the low lumen index in epiblasts and MDCK ZO1/ZO2 KO cysts. b-d. Comparison between inflation
661 response (to be completed). B. Images are shown before and after inflation. c. Change fold in the lumen
662 volume for each system, statistical test. d. Change in cell height for each system[22].

663 **Extended Figure 11: Lumen fusion dynamics in MDCK WT and ZO-KO cysts.** (a, b) ZO-KO cyst have
664 faster lumen fusion than WT in MDCK cysts with controlled initial cell number. Dynamics of MDCK WT
665 cysts (a) and ZO-KO cyst (b) with readouts of E-cadherin in green and Podocalyxin in red. The yellow line
666 outlines zones with a single lumen (8 cells WT=15; 16 cells WT=16; 8 cells ZO-KO=13; 16 cells ZO-KO=16).
667 (c) Lumen fusion comparison between MDCK WT cysts, ZO-KO cysts, and epiblasts, showing that ZO-KO
668 mutants exhibit fusion behavior similar to epiblasts. MDCK WT and ZO-KO cysts are labeled with
669 Podocalyxin (red) and E-cadherin (green), while epiblasts are stained with SiR-actin (gray). Scale bar: 10
670 µm.

671

672

673

674 **References.**

675

676 1. Zhu, M. & Zernicka-Goetz, M. Principles of Self-Organization of the Mammalian Embryo. *Cell* **183**,

677 1467–1478 (2020).

678 2. Wennekamp, S., Mesecke, S., Nédélec, F. & Hiiragi, T. A self-organization framework for symmetry
679 breaking in the mammalian embryo. *Nat Rev Mol Cell Biol* **14**, 452–459 (2013).
680 3. Hannezo, E. & Simons, B. D. Multiscale dynamics of branching morphogenesis. *Current Opinion in Cell*
681 *Biology* **60**, 99–105 (2019).
682 4. Martín-Belmonte, F. *et al.* Cell-Polarity Dynamics Controls the Mechanism of Lumen Formation in
683 Epithelial Morphogenesis. *Current Biology* **18**, 507–513 (2008).
684 5. Strilić, B. *et al.* The Molecular Basis of Vascular Lumen Formation in the Developing Mouse Aorta.
685 *Developmental Cell* **17**, 505–515 (2009).
686 6. Mangan, A. J. *et al.* Cingulin and actin mediate midbody-dependent apical lumen formation during
687 polarization of epithelial cells. *Nat Commun* **7**, 12426 (2016).
688 7. Sigurbjörnsdóttir, S., Mathew, R. & Leptin, M. Molecular mechanisms of de novo lumen formation.
689 *Nat Rev Mol Cell Biol* **15**, 665–676 (2014).
690 8. Datta, A., Bryant, D. M. & Mostov, K. E. Molecular regulation of lumen morphogenesis. *Curr Biol* **21**,
691 R126-136 (2011).
692 9. Mailleux, A. A., Overholtzer, M. & Brugge, J. S. Lumen formation during mammary epithelial
693 morphogenesis: insights from in vitro and in vivo models. *Cell Cycle* **7**, 57–62 (2008).
694 10. Dasgupta, S., Gupta, K., Zhang, Y., Viasnoff, V. & Prost, J. Physics of lumen growth. *Proc Natl*
695 *Acad Sci U S A* **115**, E4751–E4757 (2018).
696 11. Torres-Sánchez, A., Kerr Winter, M. & Salbreux, G. Tissue hydraulics: Physics of lumen formation
697 and interaction. *Cells & Development* **168**, 203724 (2021).
698 12. Dumortier, J. G. *et al.* Hydraulic fracturing and active coarsening position the lumen of the
699 mouse blastocyst. *Science* **365**, 465–468 (2019).
700 13. Li, Q. *et al.* Extracellular matrix scaffolding guides lumen elongation by inducing anisotropic
701 intercellular mechanical tension. *Nat Cell Biol* **18**, 311–318 (2016).

702 14. Ryan, A. Q., Chan, C. J., Graner, F. & Hiiragi, T. Lumen Expansion Facilitates Epiblast-Primitive
703 Endoderm Fate Specification during Mouse Blastocyst Formation. *Developmental Cell* **51**, 684-697.e4
704 (2019).
705 15. Indana, D. *et al.* Lumen expansion is initially driven by apical actin polymerization followed by
706 osmotic pressure in a human epiblast model. *Cell Stem Cell* **31**, 640-656.e8 (2024).
707 16. Chan, C. J. *et al.* Hydraulic control of mammalian embryo size and cell fate. *Nature* **571**, 112–116
708 (2019).
709 17. Villasenor, A., Chong, D. C., Henkemeyer, M. & Cleaver, O. Epithelial dynamics of pancreatic
710 branching morphogenesis. *Development* **137**, 4295–4305 (2010).
711 18. Kesavan, G. *et al.* Cdc42-Mediated Tubulogenesis Controls Cell Specification. *Cell* **139**, 791–801
712 (2009).
713 19. Chan, C. J. & Hiiragi, T. Integration of luminal pressure and signalling in tissue self-organization.
714 *Development* **147**, dev181297 (2020).
715 20. Bhat, A. *et al.* How to orient cells in microcavities for high resolution imaging of cytokinesis and
716 lumen formation. in *Methods in Cell Biology* vol. 158 25–41 (Elsevier, 2020).
717 21. Taniguchi, K. *et al.* Lumen Formation Is an Intrinsic Property of Isolated Human Pluripotent Stem
718 Cells. *Stem Cell Reports* **5**, 954–962 (2015).
719 22. Mukenhirn, M. *et al.* Tight junctions control lumen morphology via hydrostatic pressure and
720 junctional tension. *Developmental Cell* S1534580724004568 (2024)
721 doi:10.1016/j.devcel.2024.07.016.
722 23. Lee, B. H. *et al.* Control of lumen geometry and topology by the interplay between pressure and
723 cell proliferation rate in pancreatic organoids. Preprint at
724 https://doi.org/10.1101/2024.05.29.596462 (2024).

725 24. Nonomura, M. Study on Multicellular Systems Using a Phase Field Model. *PLoS ONE* **7**, e33501
726 (2012).
727 25. Akiyama, M., Nonomura, M., Tero, A. & Kobayashi, R. Numerical study on spindle positioning
728 using phase field method. *Phys. Biol.* **16**, 016005 (2018).
729 26. Tanida, S. *et al. The Interplay between Lumen Pressure and Cell Proliferation Determines*
730 *Organoid Morphology in a Multicellular Phase Field Model*.
731 http://biorxiv.org/lookup/doi/10.1101/2023.08.17.553655 (2023) doi:10.1101/2023.08.17.553655.
732 27. Harris, A. R., Daeden, A. & Charras, G. T. Formation of adherens junctions leads to the
733 emergence of a tissue-level tension in epithelial monolayers. *Journal of Cell Science* jcs.142349 (2014)
734 doi:10.1242/jcs.142349.
735 28. Comelles, J. *et al.* Epithelial colonies in vitro elongate through collective effects. *eLife* **10**, e57730
736 (2021).
737 29. Otani, T. *et al.* Claudins and JAM-A coordinately regulate tight junction formation and epithelial
738 polarity. *Journal of Cell Biology* **218**, 3372–3396 (2019).
739 30. Li, D., Mangan, A., Cicchini, L., Margolis, B. & Prekeris, R. FIP 5 phosphorylation during mitosis
740 regulates apical trafficking and lumenogenesis. *EMBO Rep* **15**, 428–437 (2014).
741 31. Zieger, E. *et al.* Midbody-Localized Aquaporin Mediates Intercellular Lumen Expansion During
742 Early Cleavage of an Invasive Freshwater Bivalve. *Front. Cell Dev. Biol.* **10**, 894434 (2022).
743 32. Zhang, Y. *et al.* Biomimetic niches reveal the minimal cues to trigger apical lumen formation in
744 single hepatocytes. *Nat. Mater.* **19**, 1026–1035 (2020).
745 33. Shahbazi, M. N. *et al.* Pluripotent state transitions coordinate morphogenesis in mouse and
746 human embryos. *Nature* **552**, 239–243 (2017).
747 34. Kim, Y. S. *et al.* Deciphering epiblast lumenogenesis reveals proamniotic cavity control of
748 embryo growth and patterning. *Sci. Adv.* **7**, eabe1640 (2021).

749 35. Alvers, A. L., Ryan, S., Scherz, P. J., Huisken, J. & Bagnat, M. Single continuous lumen formation
750 in the zebrafish gut is mediated by *smoothened* -dependent tissue remodeling. *Development* **141**,
751 1110–1119 (2014).
752 36. Bagnat, M., Cheung, I. D., Mostov, K. E. & Stainier, D. Y. R. Genetic control of single lumen
753 formation in the zebrafish gut. *Nat Cell Biol* **9**, 954–960 (2007).
754 37. Carleton, A. E., Duncan, M. C. & Taniguchi, K. Human epiblast lumenogenesis: From a cell
755 aggregate to a lumenal cyst. *Seminars in Cell & Developmental Biology* **131**, 117–123 (2022).
756 38. Dahl-Jensen, S. B. *et al.* Deconstructing the principles of ductal network formation in the
757 pancreas. *PLoS Biol* **16**, e2002842 (2018).
758 39. Gonay, L. *et al.* Modelling of Epithelial Growth, Fission and Lumen Formation During Embryonic
759 Thyroid Development: A Combination of Computational and Experimental Approaches. *Front.*
760 *Endocrinol.* **12**, 655862 (2021).
761 40. Bedzhov, I. & Zernicka-Goetz, M. Self-Organizing Properties of Mouse Pluripotent Cells Initiate
762 Morphogenesis upon Implantation. *Cell* **156**, 1032–1044 (2014).
763 41. Noor, N. *et al.* 3D Printing of Personalized Thick and Perfusable Cardiac Patches and Hearts.
764 *Advanced Science* **6**, 1900344 (2019).
765 42. Jorgensen, A. M. *et al.* Multicellular bioprinted skin facilitates human-like skin architecture in
766 vivo. *Sci. Transl. Med.* **15**, eadf7547 (2023).
767 43. Martin-Lemaitre, C., Alcheikh, Y., Naumann, R. & Honigmann, A. *Optimization of Mouse*
768 *Embryonic Stem Cell Culture for Organoid and Chimeric Mice Production*.
769 http://biorxiv.org/lookup/doi/10.1101/2020.03.13.990135 (2020) doi:10.1101/2020.03.13.990135.
770 44. Greggio, C., De Franceschi, F., Figueiredo-Larsen, M. & Grapin-Botton, A. In Vitro Pancreas
771 Organogenesis from Dispersed Mouse Embryonic Progenitors. *JoVE* 51725 (2014) doi:10.3791/51725.

45. Lu, L. *et al. Polarity-Driven Three-Dimensional Spontaneous Rotation of a Cell Doublet*. http://biorxiv.org/lookup/doi/10.1101/2022.12.21.521355 (2022) doi:10.1101/2022.12.21.521355.

46. Balasubramaniam, L. *et al.* Investigating the nature of active forces in tissues reveals how contractile cells can form extensile monolayers. *Nat. Mater.* **20**, 1156–1166 (2021).

47. Wollrab, V., Thiagarajan, R., Wald, A., Kruse, K. & Riveline, D. Still and rotating myosin clusters determine cytokinetic ring constriction. *Nat Commun* **7**, 11860 (2016).

48. Greggio, C. *et al.* Artificial three-dimensional niches deconstruct pancreas development *in vitro*. *Development* **140**, 4452–4462 (2013).

49. Guevorkian, K. & Maître, J.-L. Micropipette aspiration. in *Methods in Cell Biology* vol. 139 187–201 (Elsevier, 2017).

50. Ahrens, J., Geveci, B. & Law, C. ParaView: An End-User Tool for Large-Data Visualization. in *Visualization Handbook* 717–731 (Elsevier, 2005). doi:10.1016/B978-012387582-2/50038-1.

51. Olsson, E. & Kreiss, G. A conservative level set method for two phase flow. *Journal of Computational Physics* **210**, 225–246 (2005).

52. Badillo, A. Quantitative phase-field modeling for boiling phenomena. *Phys. Rev. E* **86**, 041603 (2012).

Figure 1

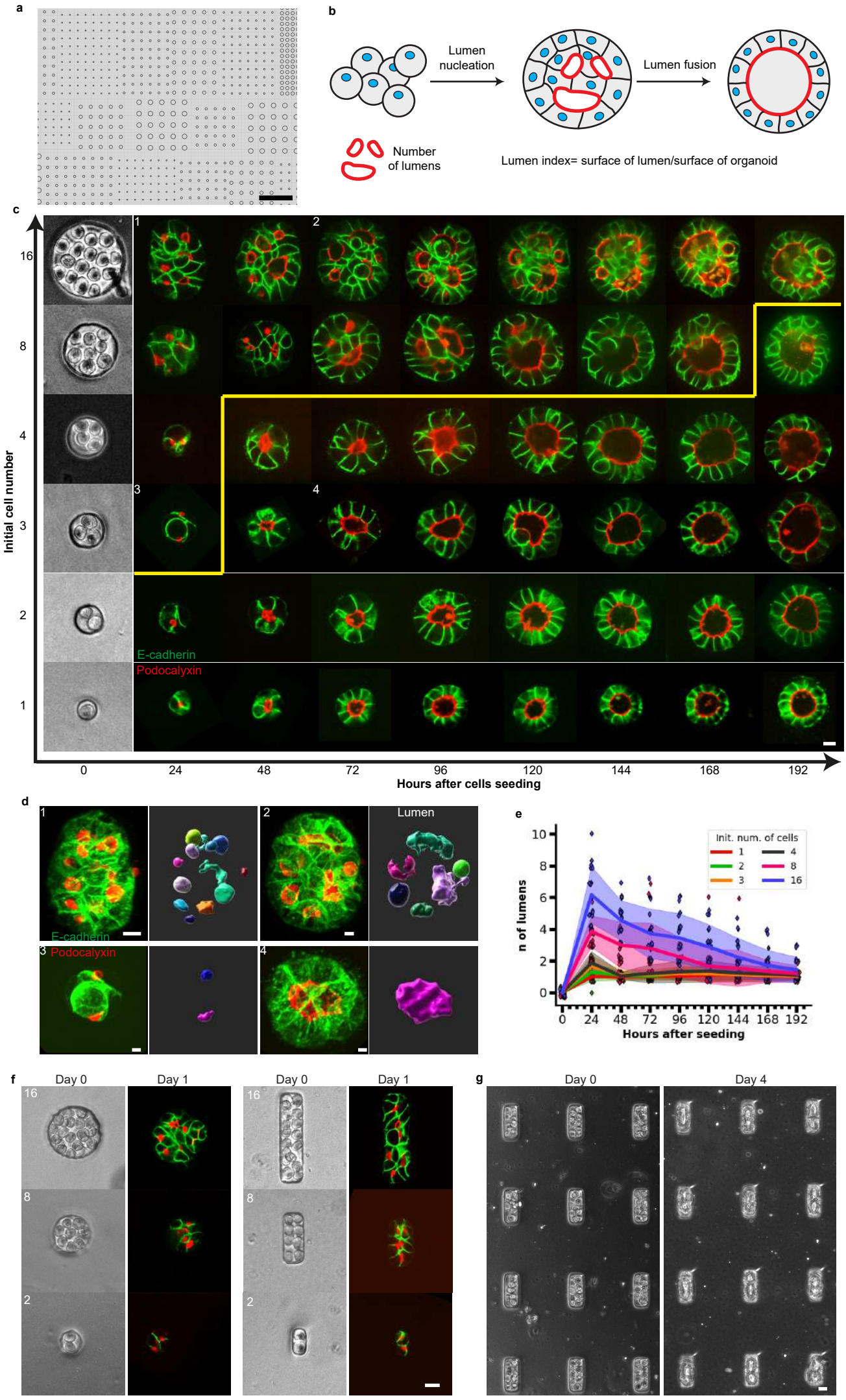
a
b
Lumen nucleation
Lumen fusion
Number of lumens
Lumen index= surface of lumen/surface of organoid
c
Initial cell number
16
8
4
3
2
1
E-cadherin
Podocalyxin
0
24
48
72
96
120
144
168
192
Hours after cells seeding
d
E-cadherin
Podocalyxin
Lumen
e
Init. num. of cells
1
2
3
4
8
16
n of lumens
Hours after seeding
f
Day 0
Day 1
g
Day 0
Day 4

Figure 2

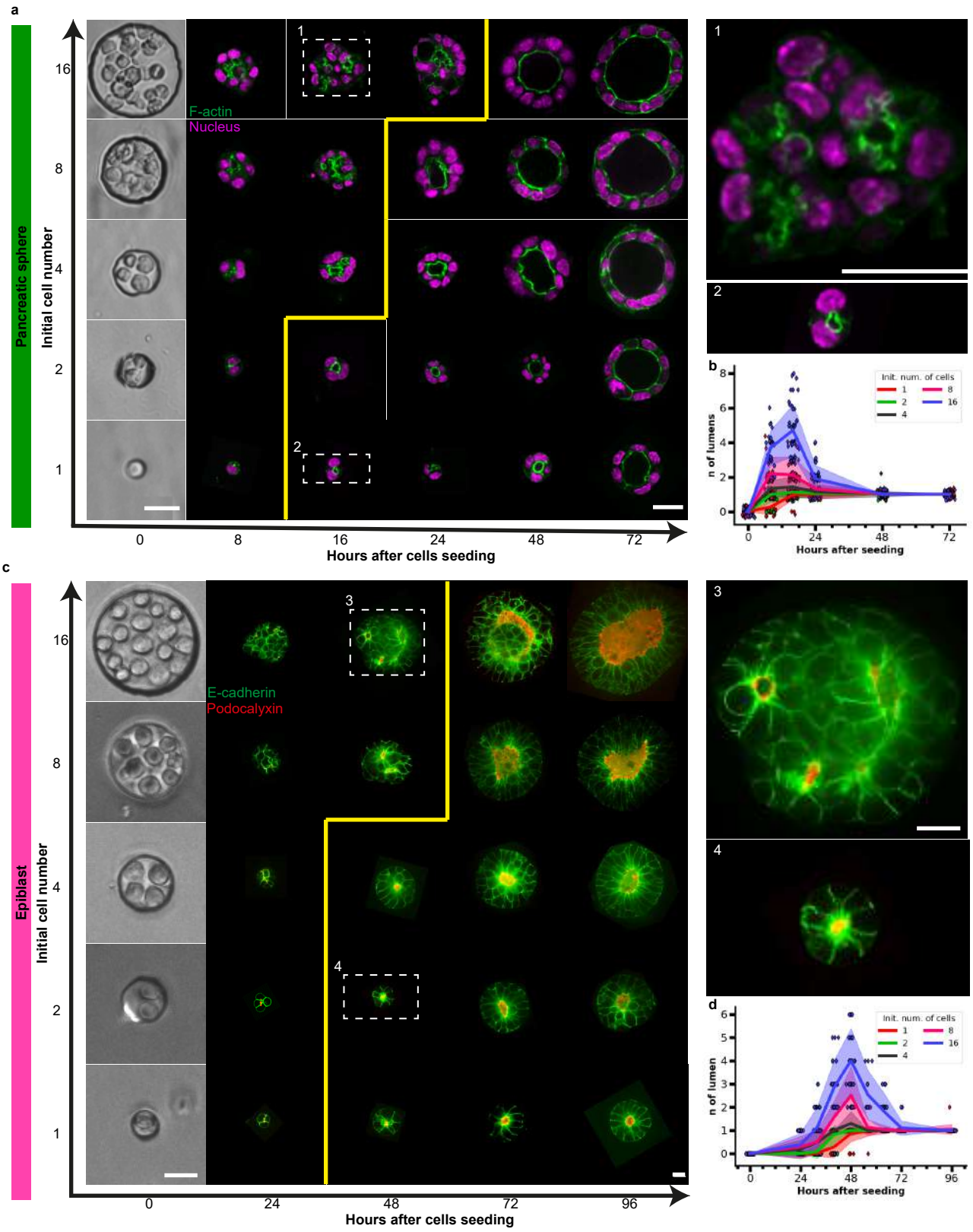
a
Pancreatic sphere
Initial cell number
16
8
4
2
1
F-actin
Nucleus
1
2
0
8
16
24
48
72
Hours after cells seeding
b
n of lumens
Init. num. of cells
1
2
4
8
16
Hours after seeding
c
Epiblast
Initial cell number
E-cadherin
Podocalyxin
3
4
0
24
48
72
96
Hours after cells seeding
d
n of lumen
Hours after seeding

Figure 3

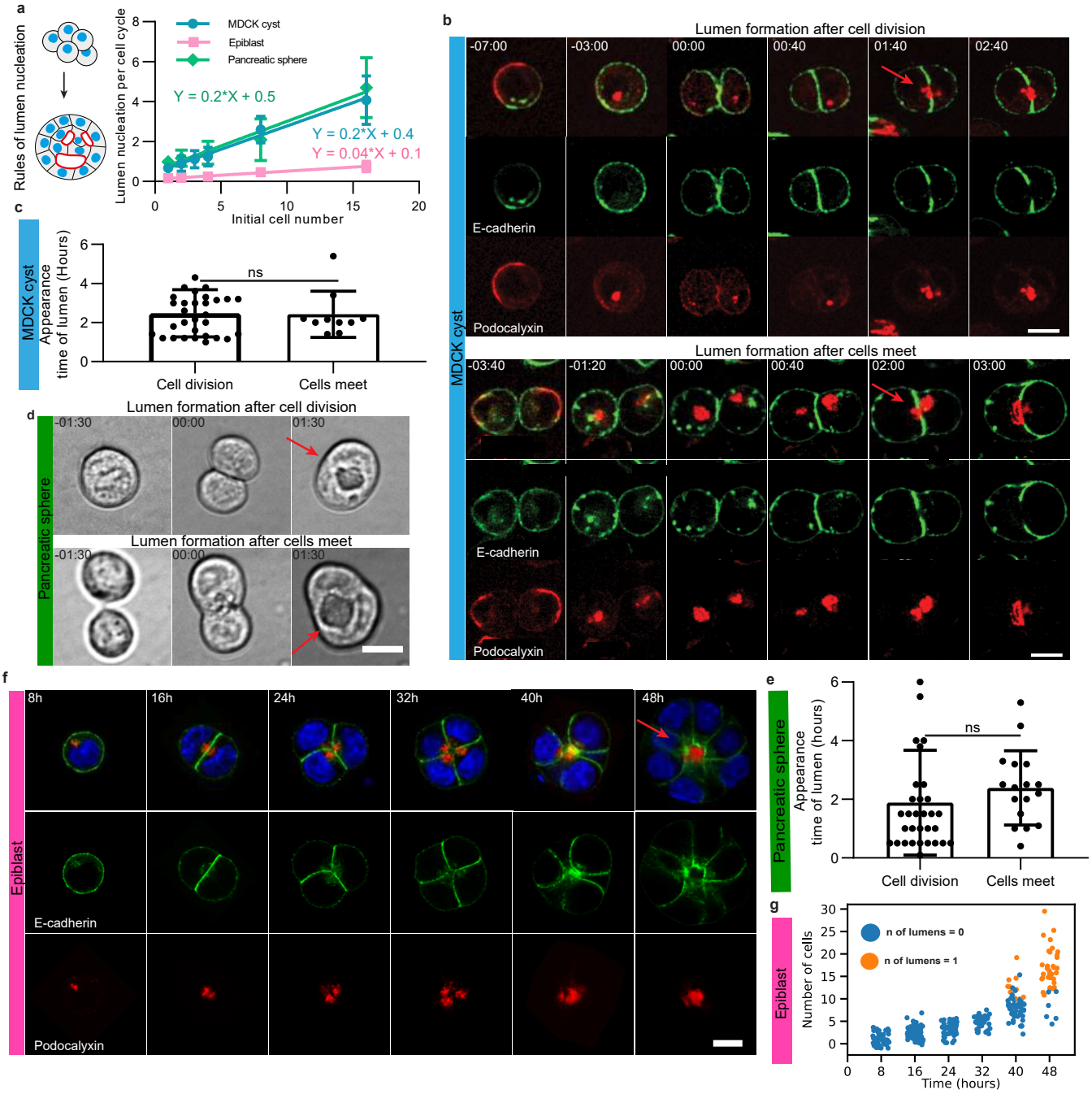
a
Rules of lumen nucleation
Lumen nucleation per cell cycle
MDCK cyst
Epiblast
Pancreatic sphere
Y = 0.2*X + 0.5
Y = 0.2*X + 0.4
Y = 0.04*X + 0.1
Initial cell number
b
Lumen formation after cell division
-07:00
-03:00
00:00
00:40
01:40
02:40
E-cadherin
Podocalyxin
MDCK cyst
Lumen formation after cells meet
-03:40
-01:20
00:00
00:40
02:00
03:00
E-cadherin
Podocalyxin
c
MDCK cyst
Appearance time of lumen (Hours)
ns
Cell division
Cells meet
d
Pancreatic sphere
Lumen formation after cell division
-01:30
00:00
01:30
Lumen formation after cells meet
-01:30
00:00
01:30
e
Pancreatic sphere
Appearance time of lumen (hours)
ns
Cell division
Cells meet
f
Epiblast
8h
16h
24h
32h
40h
48h
E-cadherin
Podocalyxin
g
Epiblast
Number of cells
n of lumens = 0
n of lumens = 1
Time (hours)

Figure 4

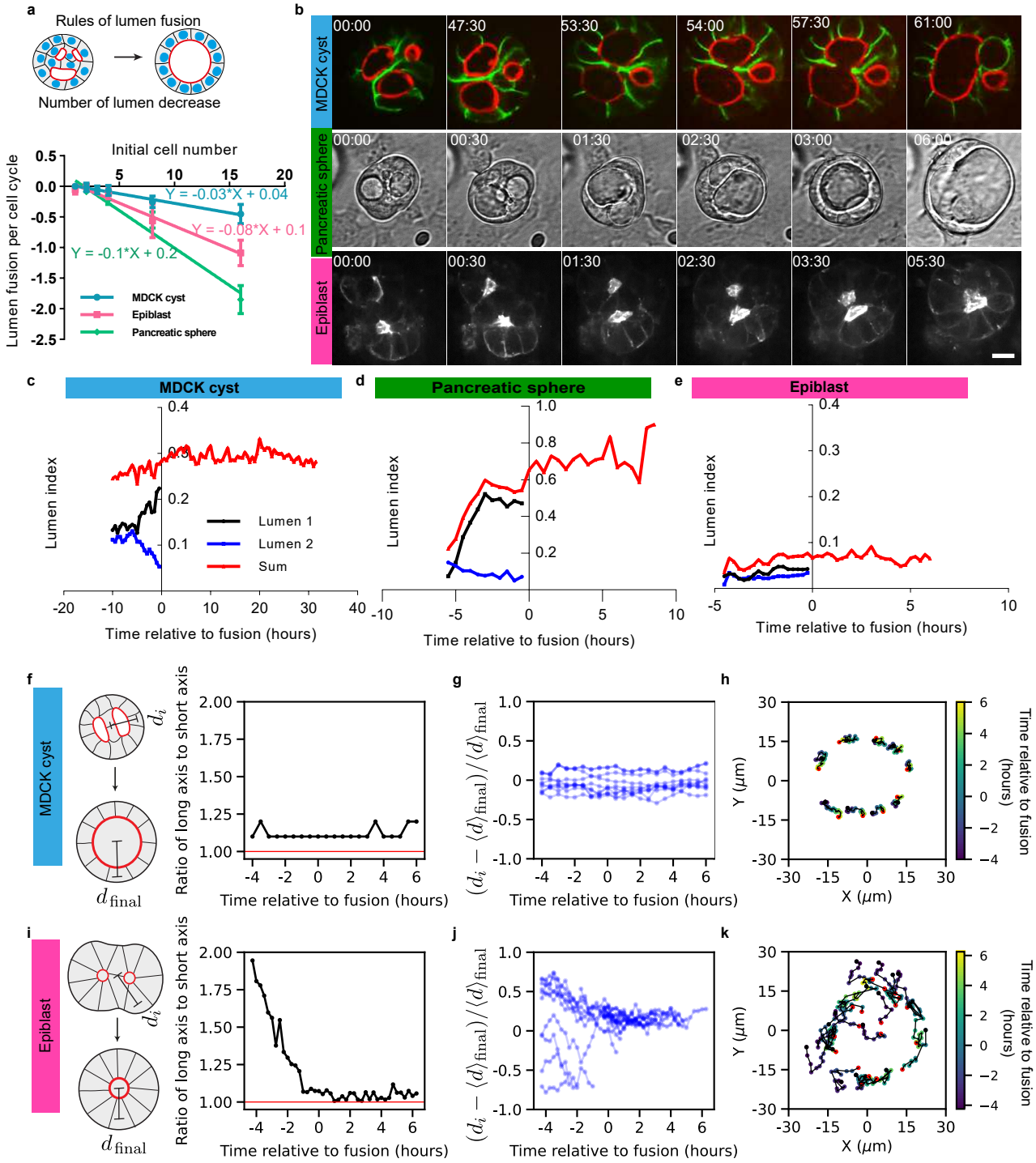
a
Rules of lumen fusion
Number of lumen decrease
Initial cell number
Lumen fusion per cell cycle
Y = -0.03*X + 0.04
Y = -0.08*X + 0.1
Y = -0.1*X + 0.2
MDCK cyst
Epiblast
Pancreatic sphere
b
MDCK cyst
Pancreatic sphere
Epiblast
00:00
47:30
53:30
54:00
57:30
61:00
00:30
01:30
02:30
03:00
06:00
03:30
05:30
c
MDCK cyst
d
Pancreatic sphere
e
Epiblast
Lumen index
Lumen 1
Lumen 2
Sum
Time relative to fusion (hours)
f
MDCK cyst
d_i
d_{final}
Ratio of long axis to short axis
g
$(d_i - \langle d \rangle_{\mathrm{final}}) / \langle d \rangle_{\mathrm{final}}$
h
Y (μm)
X (μm)
Time relative to fusion (hours)
i
Epiblast
j
k

Figure 5

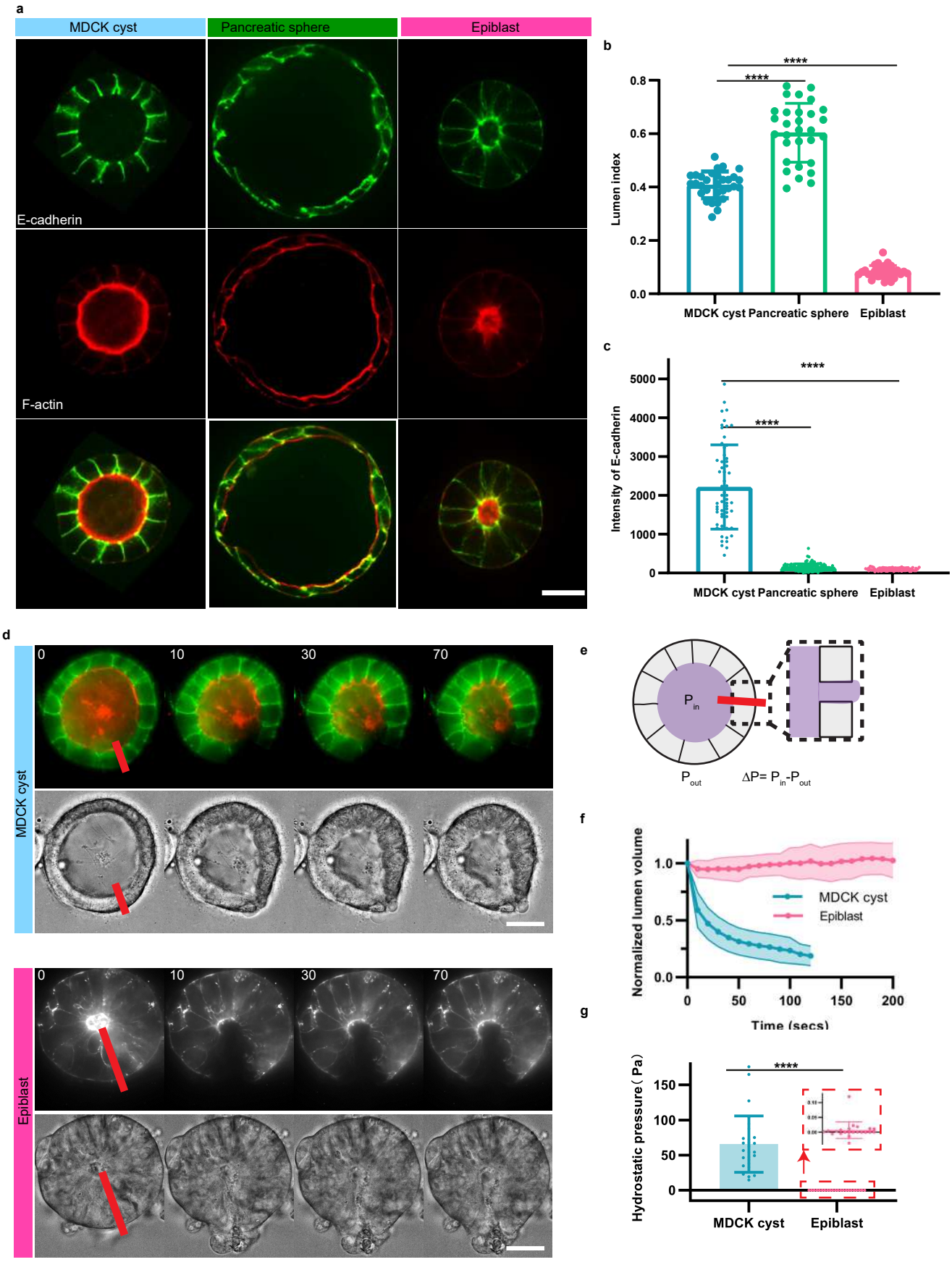
a
MDCK cyst
Pancreatic sphere
Epiblast
E-cadherin
F-actin
b
Lumen index
0.8
0.6
0.4
0.2
0.0
****
****
MDCK cyst
Pancreatic sphere
Epiblast
c
Intensity of E-cadherin
5000
4000
3000
2000
1000
0
****
****
MDCK cyst
Pancreatic sphere
Epiblast
d
MDCK cyst
0
10
30
70
Epiblast
0
10
30
70
e
P_{in}
P_{out}
$\Delta P = P_{in} - P_{out}$
f
Normalized lumen volume
1.0
0.5
0.0
MDCK cyst
Epiblast
0
50
100
150
200
Time (secs)
g
Hydrostatic pressure (Pa)
150
100
50
0
****
MDCK cyst
Epiblast

Figure 6

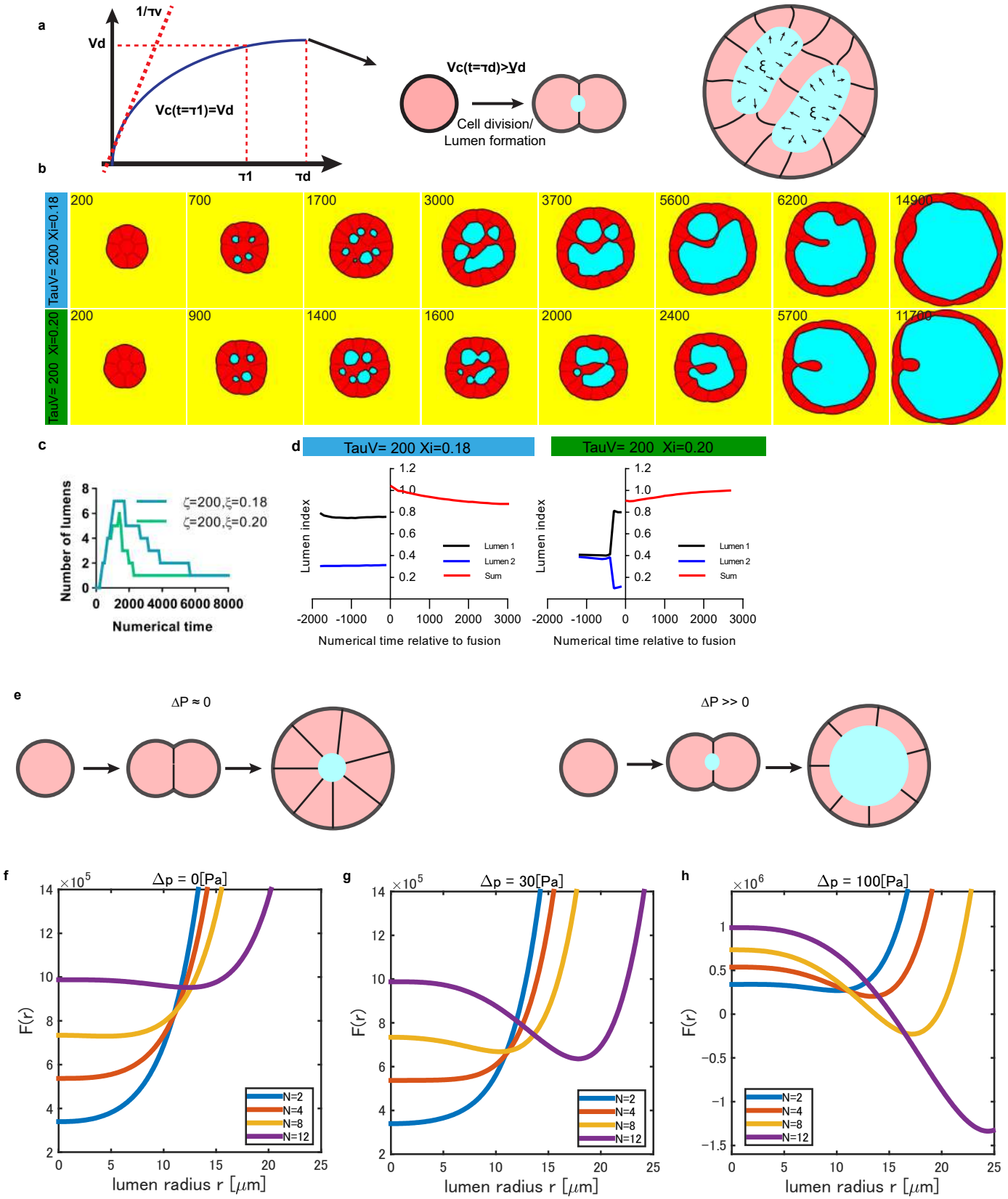
a
1/τv
Vd
Vc(t=τ1)=Vd
τ1
τd
Vc(t=τd)>Vd
Cell division/
Lumen formation
ξ
ξ
b
TauV= 200 Xi=0.18
200
700
1700
3000
3700
5600
6200
14900
TauV= 200 Xi=0.20
200
900
1400
1600
2000
2400
5700
11700
c
Number of lumens
ζ=200,ξ=0.18
ζ=200,ξ=0.20
Numerical time
d
TauV= 200 Xi=0.18
TauV= 200 Xi=0.20
Lumen index
Lumen 1
Lumen 2
Sum
Numerical time relative to fusion
e
ΔP ≈ 0
ΔP >> 0
f
Δp = 0[Pa]
F(r)
N=2
N=4
N=8
N=12
lumen radius r [μm]
g
Δp = 30[Pa]
h
Δp = 100[Pa]

Figure 7

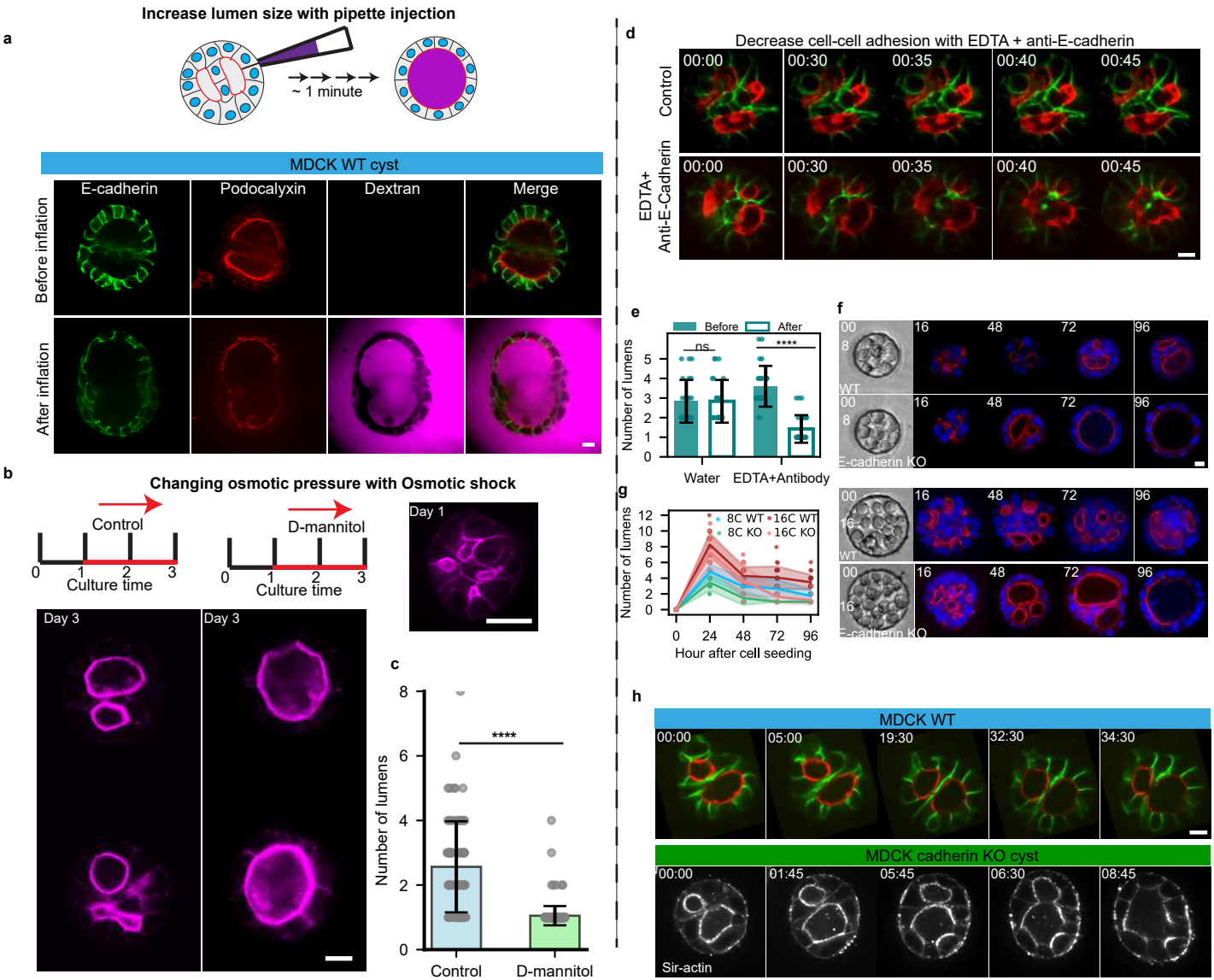
a
Increase lumen size with pipette injection
~ 1 minute
MDCK WT cyst
E-cadherin
Podocalyxin
Dextran
Merge
Before inflation
After inflation
b
Changing osmotic pressure with Osmotic shock
Control
D-mannitol
Culture time
Day 1
Day 3
Day 3
c
Number of lumens
****
Control
D-mannitol
d
Decrease cell-cell adhesion with EDTA + anti-E-cadherin
Control
EDTA+ Anti-E-Cadherin
00:00
00:30
00:35
00:40
00:45
e
Before
After
ns
****
Number of lumens
Water
EDTA+Antibody
f
WT
E-cadherin KO
16
48
72
96
g
8C WT
16C WT
8C KO
16C KO
Number of lumens
Hour after cell seeding
h
MDCK WT
00:00
05:00
19:30
32:30
34:30
MDCK cadherin KO cyst
01:45
05:45
06:30
08:45
Sir-actin

Figure 8

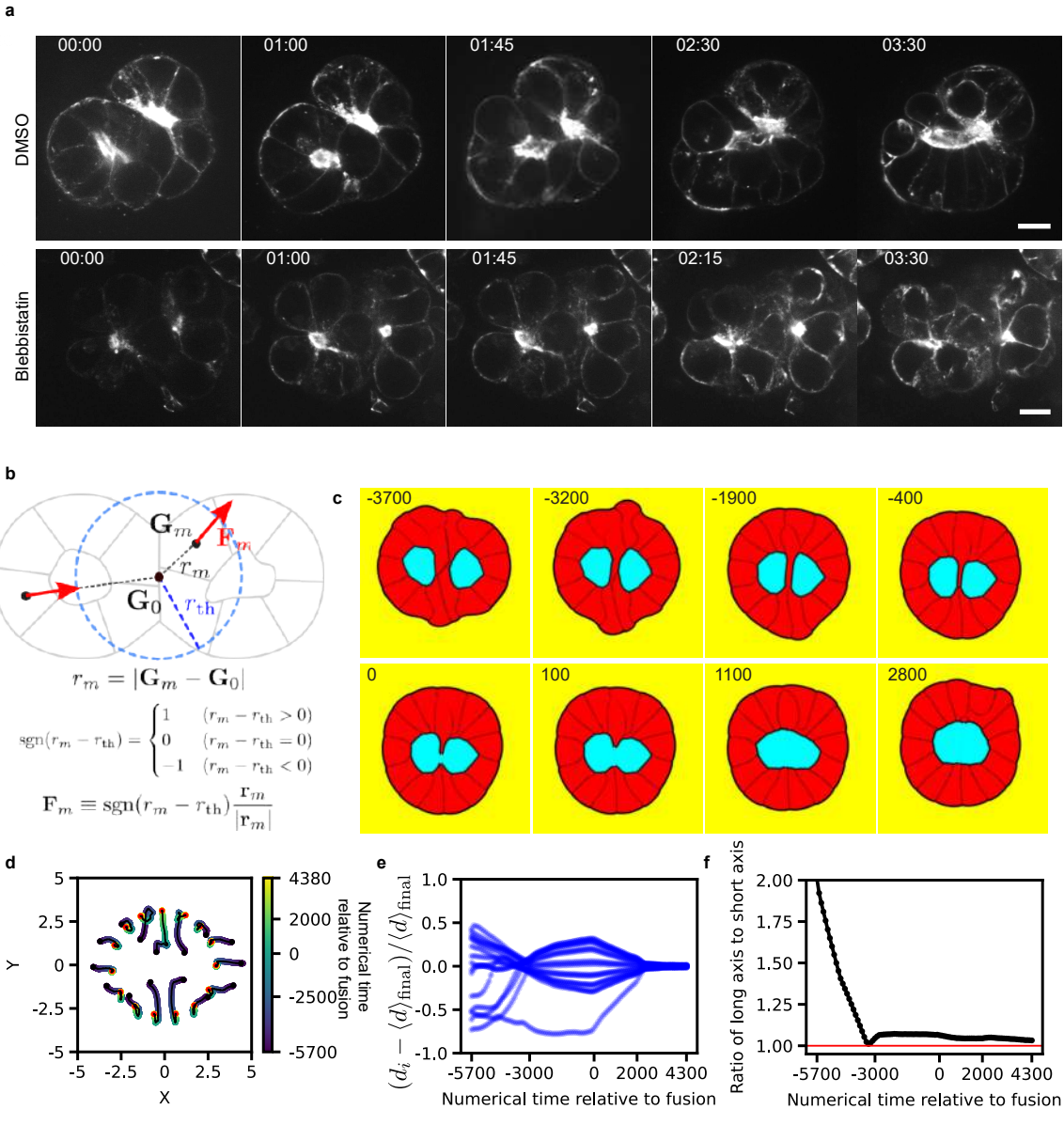
a
DMSO
00:00
01:00
01:45
02:30
03:30
Blebbistatin
00:00
01:00
01:45
02:15
03:30
b
$\mathbf{G}_m$
$\mathbf{F}_m$
r_m
$\mathbf{G}_0$
r_{th}
$r_m = |\mathbf{G}_m - \mathbf{G}_0|$
$\mathrm{sgn}(r_m - r_{\mathrm{th}}) = \begin{cases} 1 & (r_m - r_{\mathrm{th}} > 0) \\ 0 & (r_m - r_{\mathrm{th}} = 0) \\ -1 & (r_m - r_{\mathrm{th}} < 0) \end{cases}$
$\mathbf{F}_m \equiv \mathrm{sgn}(r_m - r_{\mathrm{th}}) \frac{\mathbf{r}_m}{|\mathbf{r}_m|}$
c
-3700
-3200
-1900
-400
0
100
1100
2800
d
Y
X
Numerical time relative to fusion
e
$(d_i - \langle d \rangle_{\mathrm{final}}) / \langle d \rangle_{\mathrm{final}}$
Numerical time relative to fusion
f
Ratio of long axis to short axis
Numerical time relative to fusion

Figure 9

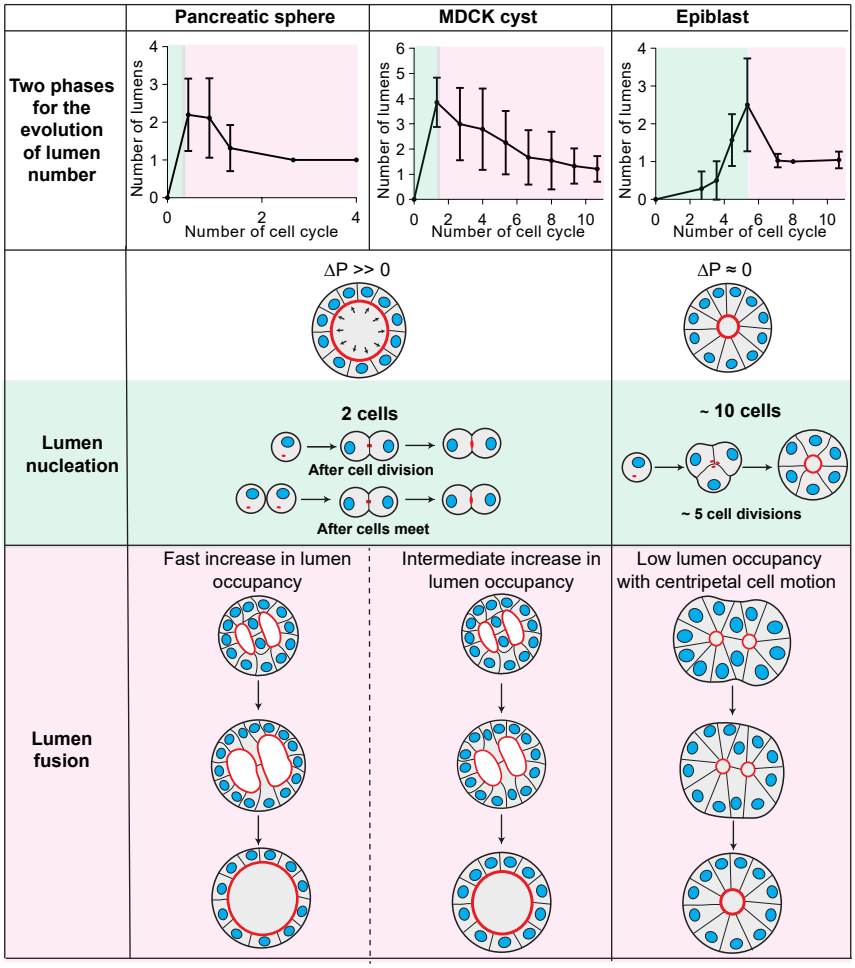
Pancreatic sphere
MDCK cyst
Epiblast
Two phases for the evolution of lumen number
Number of lumens
Number of cell cycle
ΔP >> 0
ΔP ≈ 0
Lumen nucleation
2 cells
After cell division
After cells meet
~ 10 cells
~ 5 cell divisions
Lumen fusion
Fast increase in lumen occupancy
Intermediate increase in lumen occupancy
Low lumen occupancy with centripetal cell motion

Extended Figure 1

a

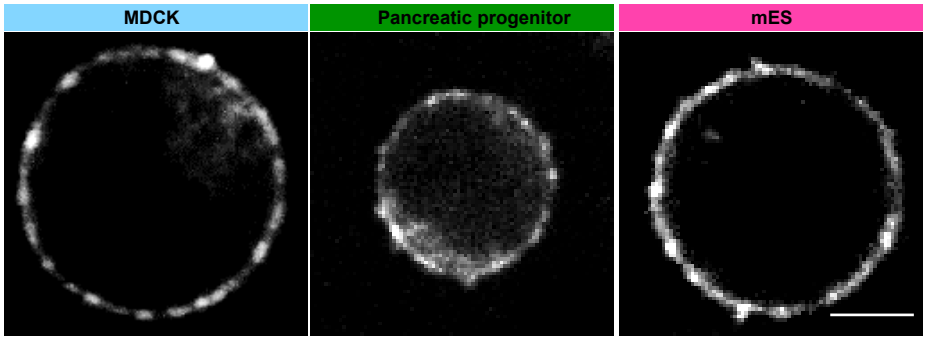

b

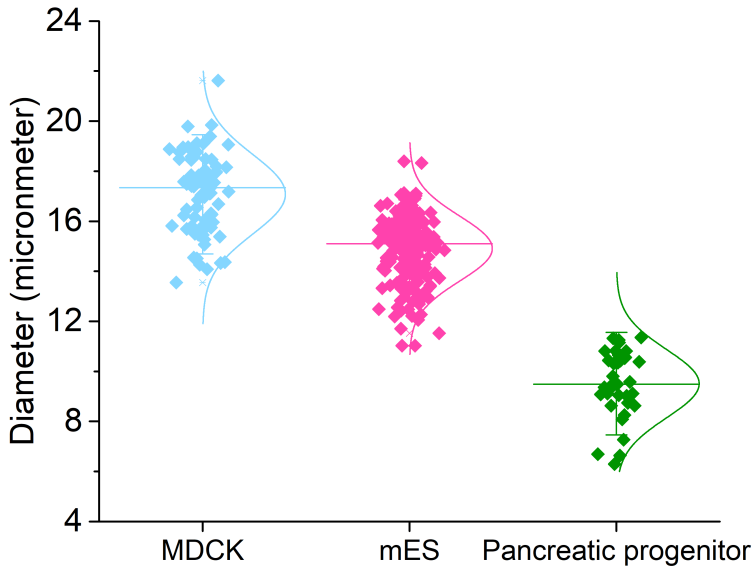

c

Initial cell numbers	MDCK cyst	Pancreatic sphere	Epiblast
	Diameter of cavities (μm)		
1	17.5	10	15
2	25	14	21
3	30	-	-
4	35	20	30
8	50	30	42
16	70	40	60

Extended Figure 2

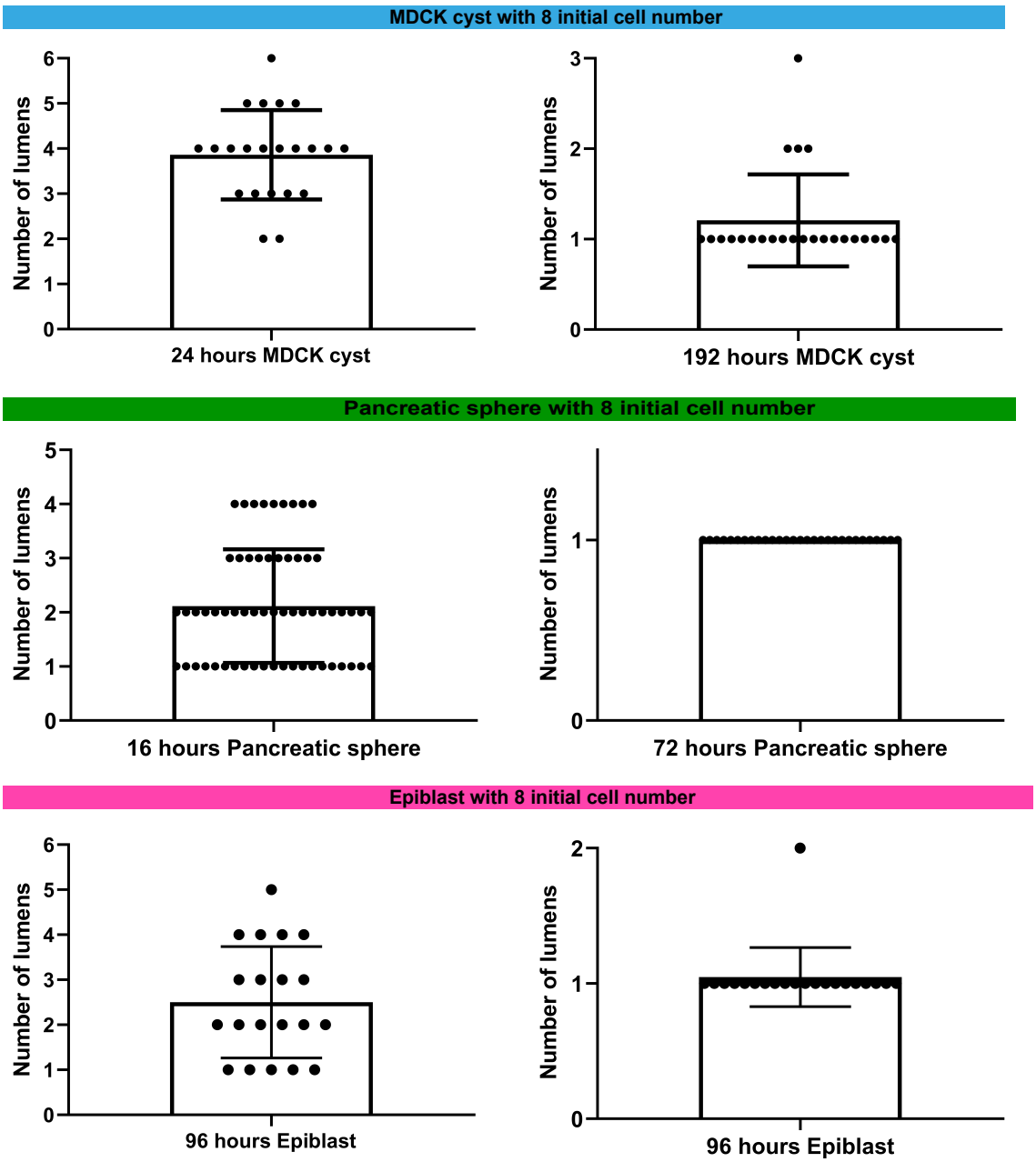

Extended Figure 3

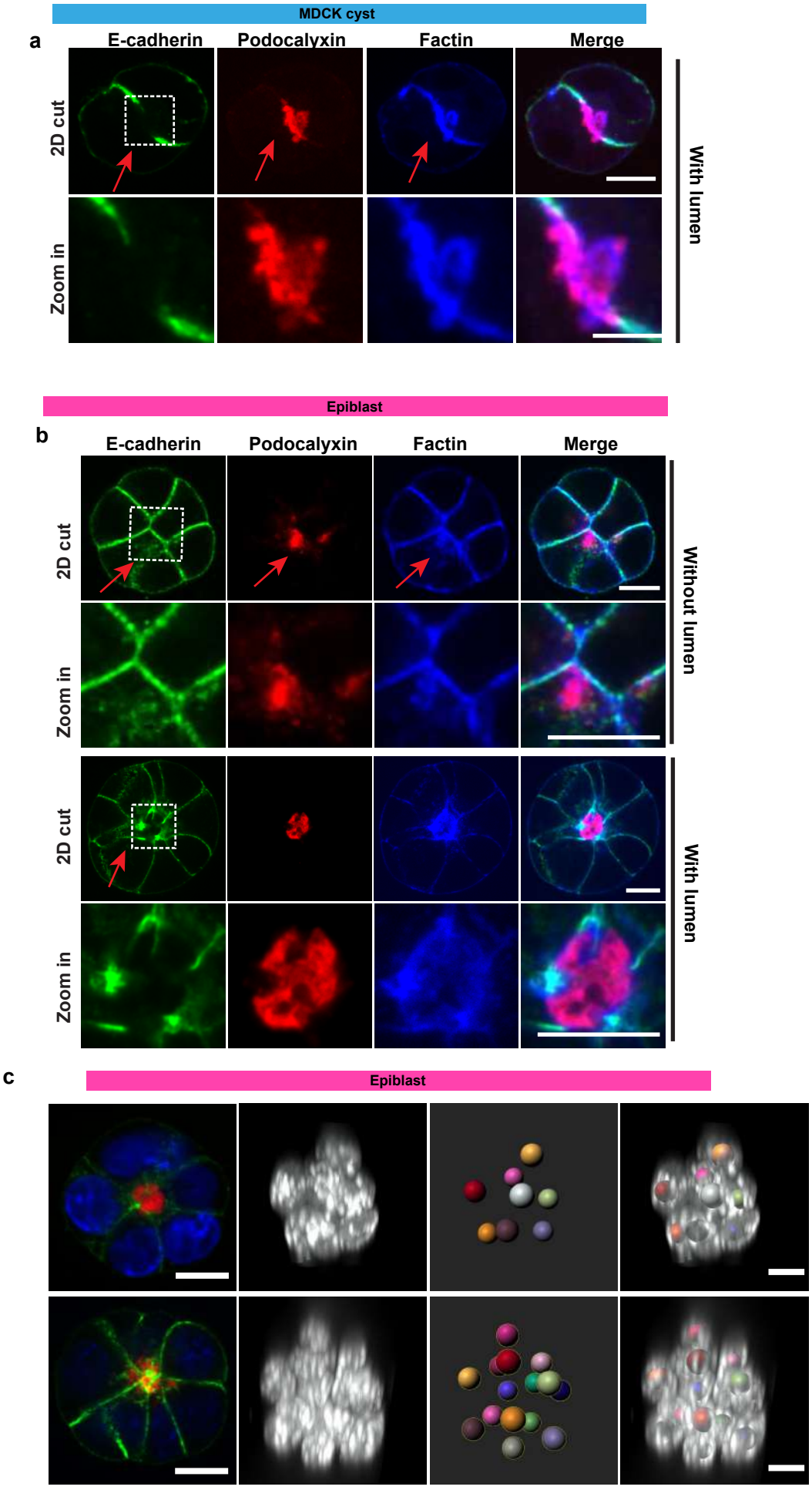

Extended Figure 4

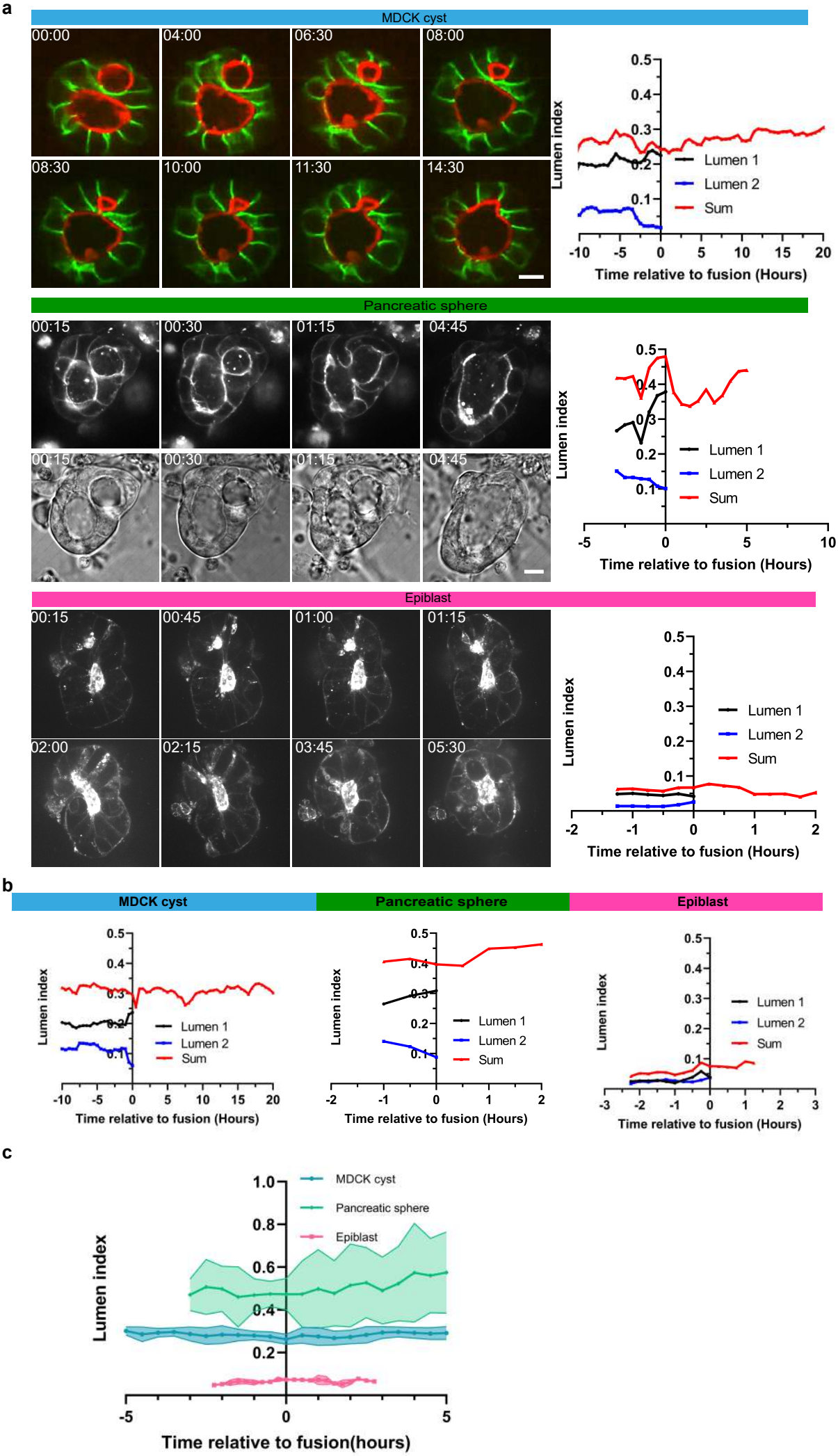

Extended Figure 5

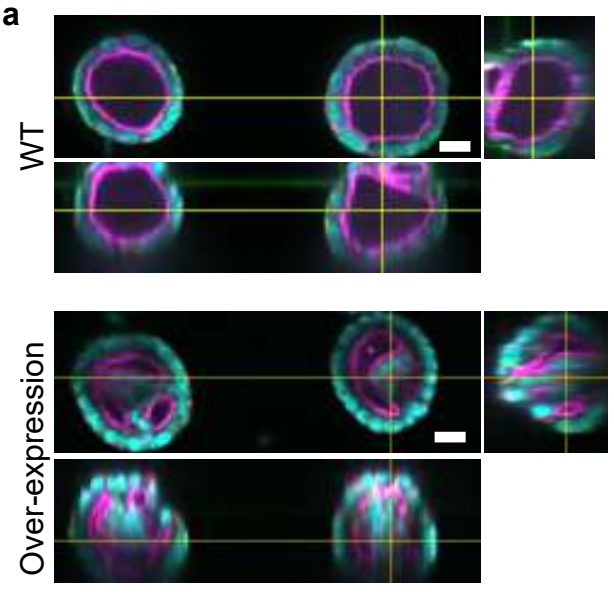

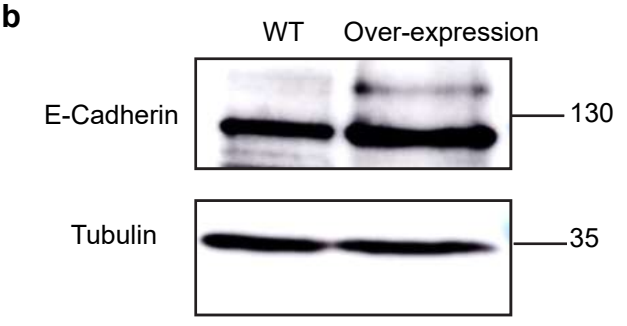

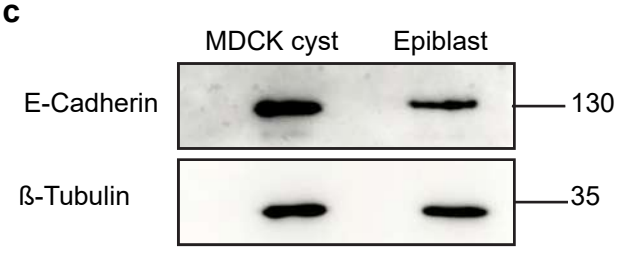

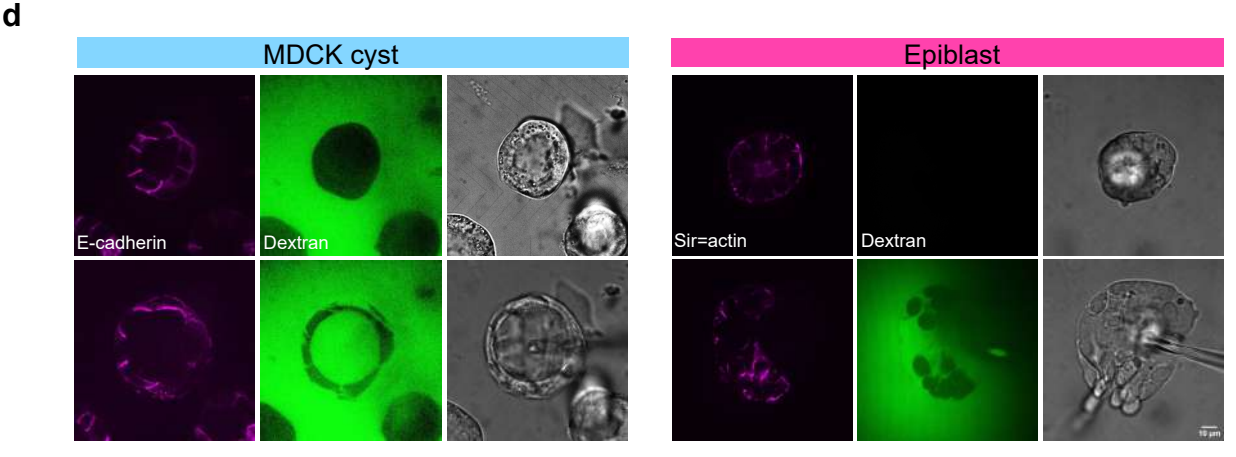

Extended Figure 6

a

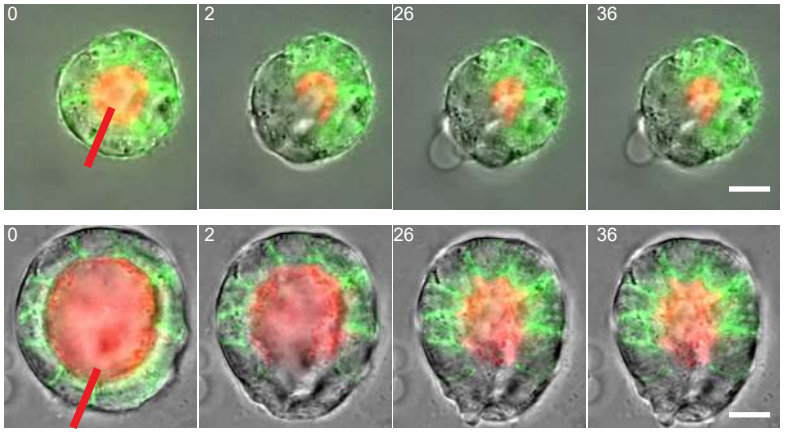

b

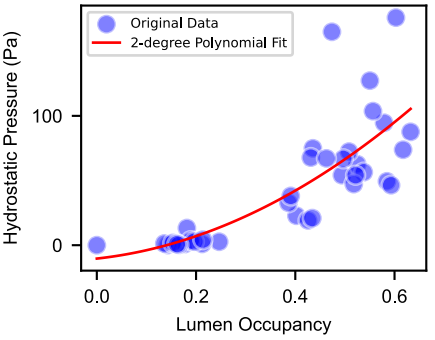

c

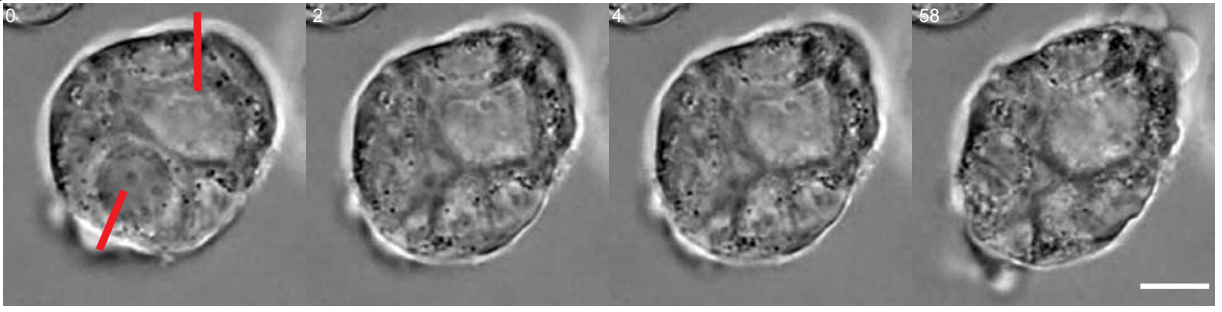

d

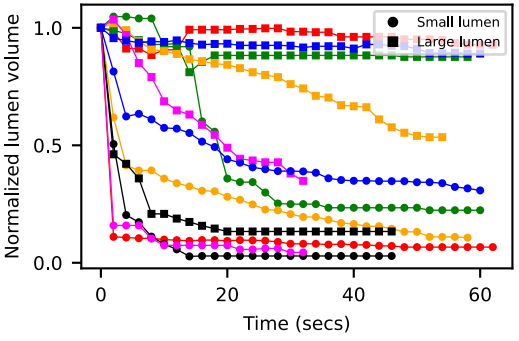

e

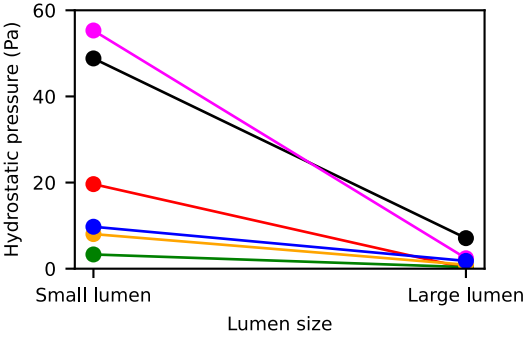

Extended Figure 7

a

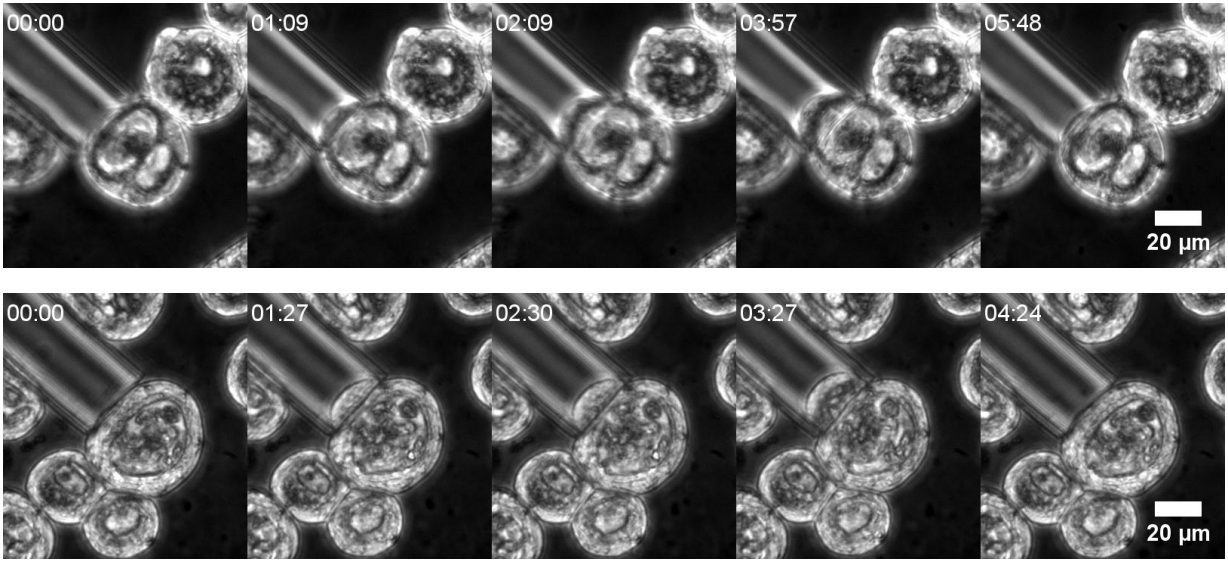

b

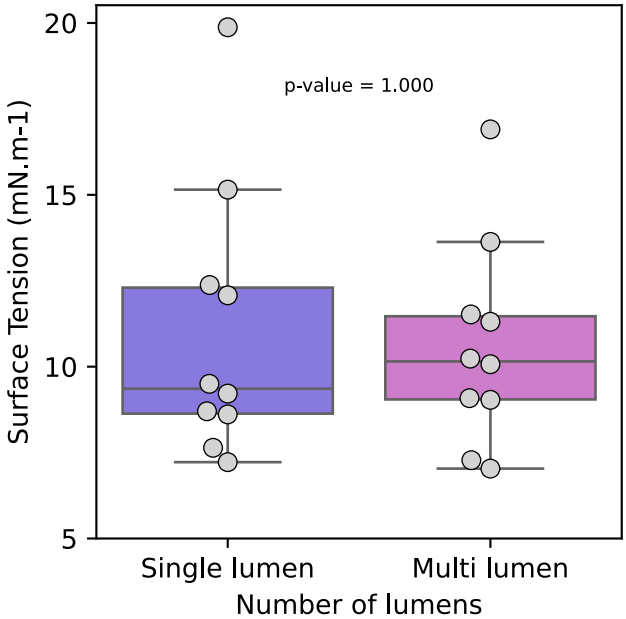

Extended Figure 8

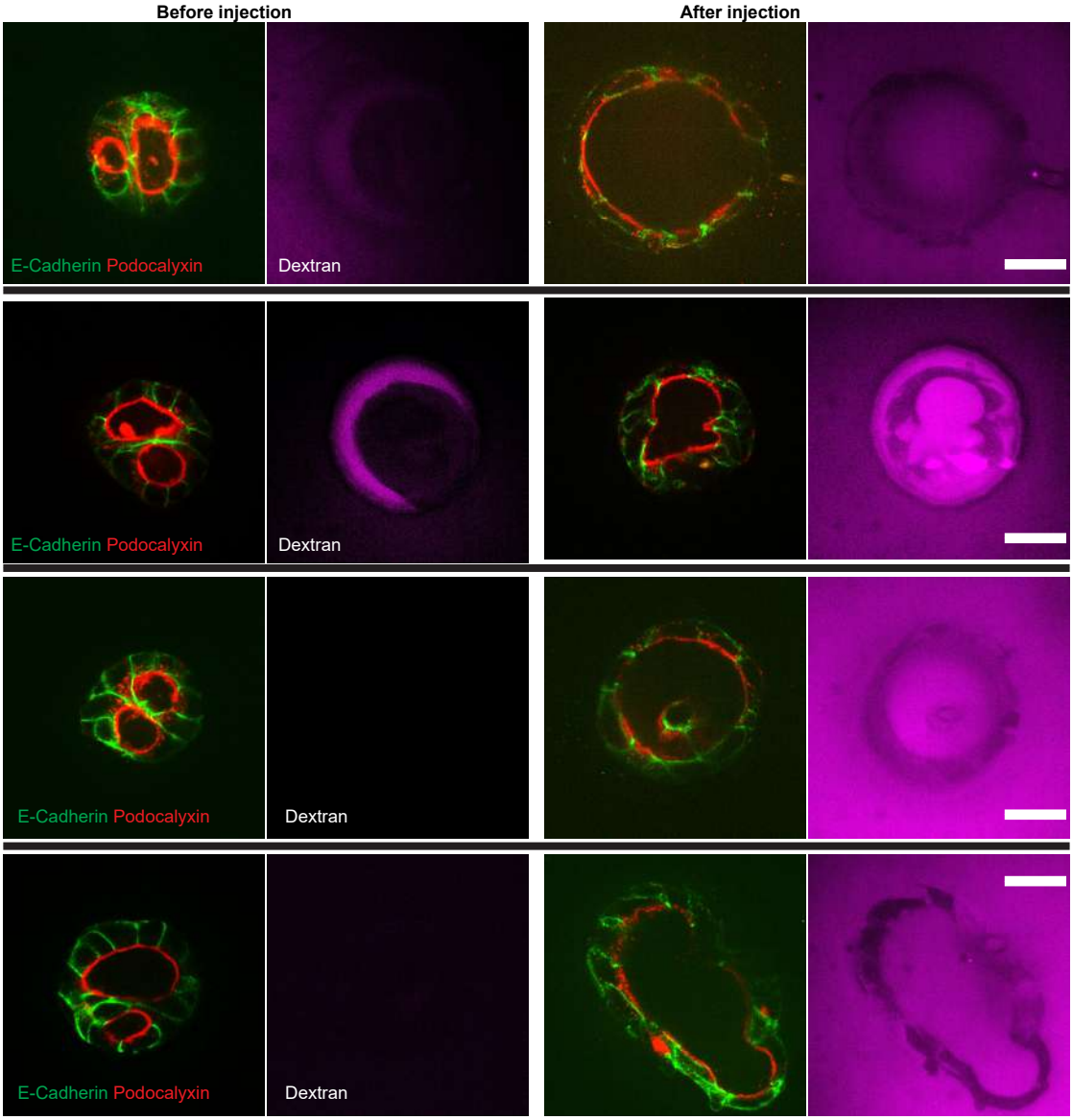

Extended Figure 9

a

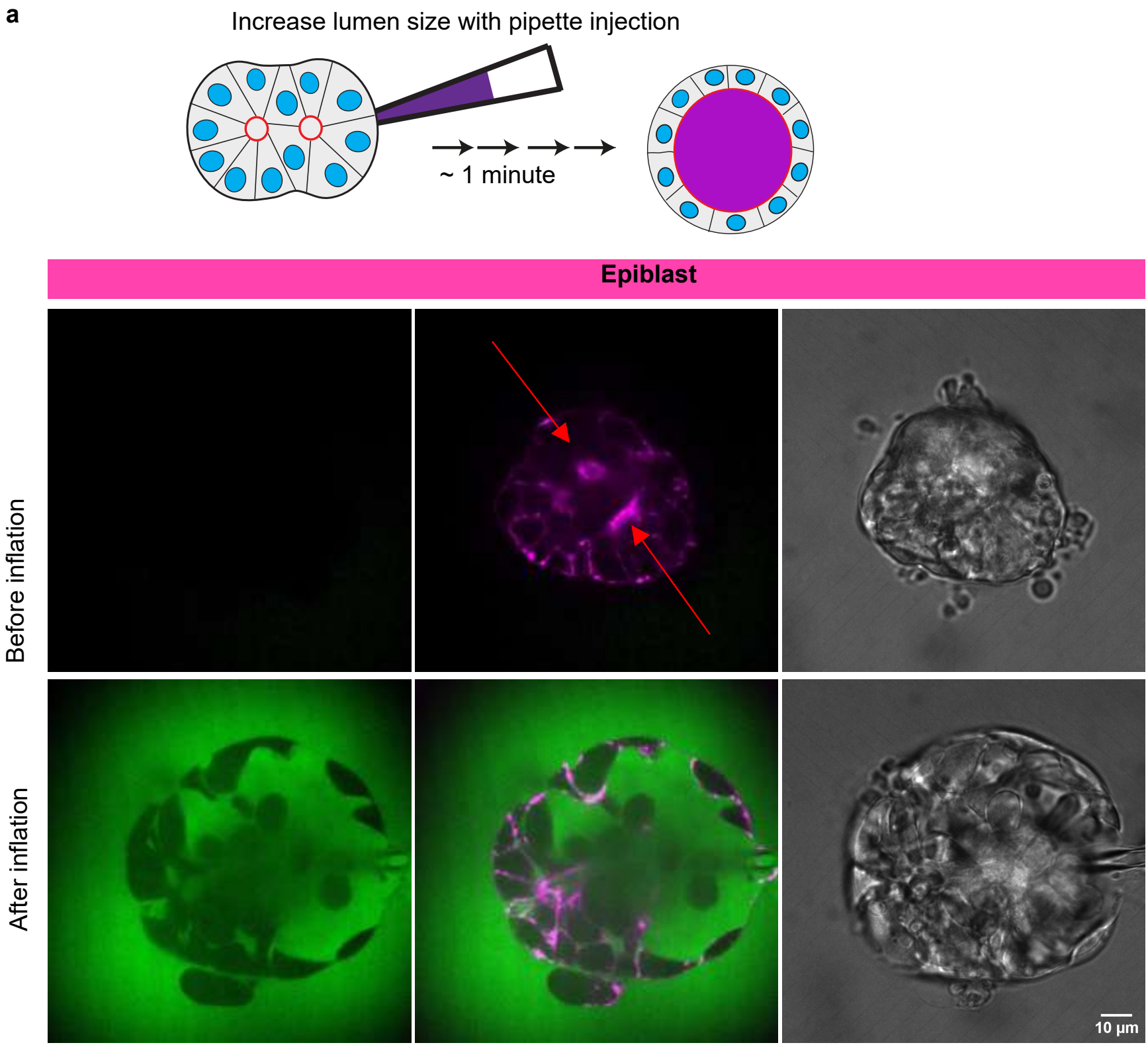

Extended Figure 10

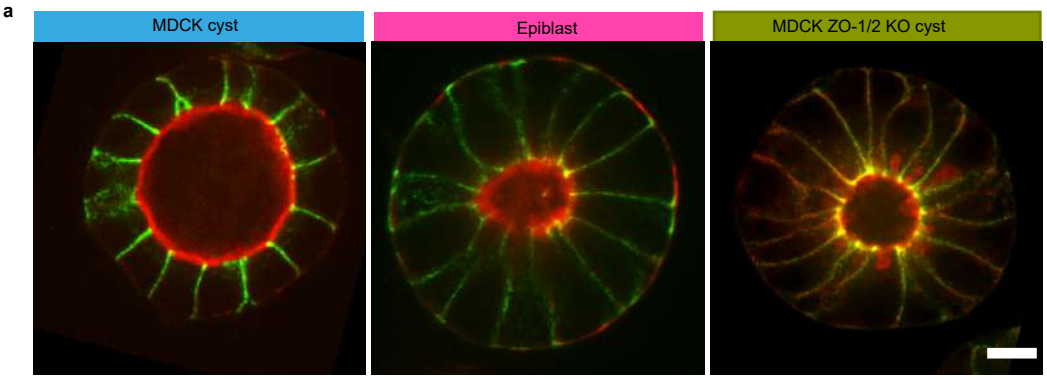

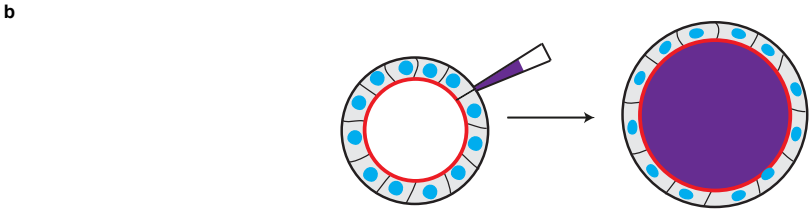

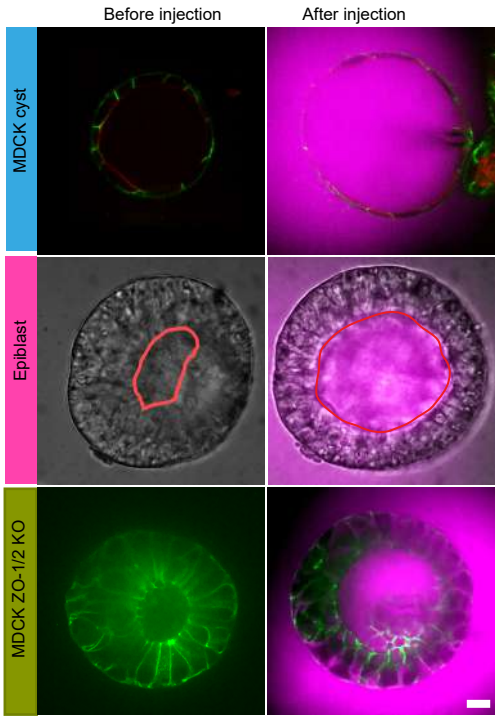

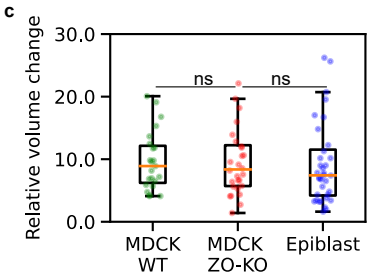

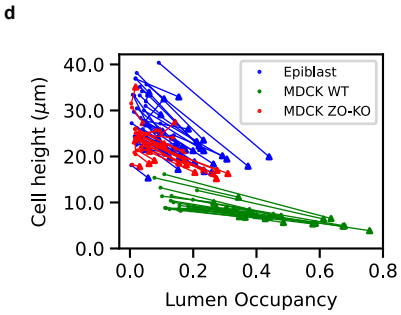

Extended Figure 11
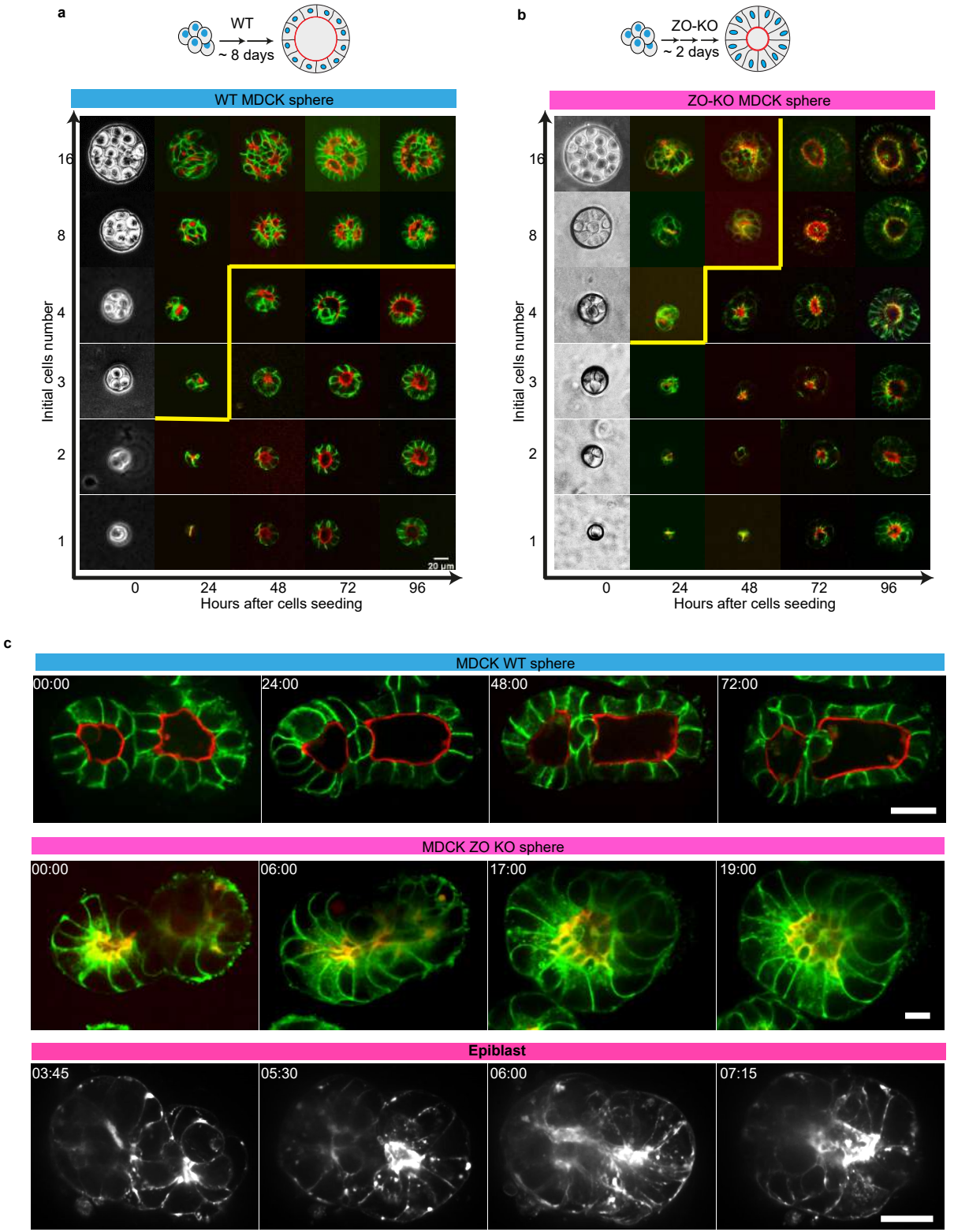
Change lumen dynamics by change cellular properties